Journal of Energy Chemistry 31 (2019) 54–78

Contents lists available at ScienceDirect

Journal of Energy Chemistry

journal homepage: www.elsevier.com/locate/jechem

http://www.journals.elsevier.com/journal-of-energy-chemistry/

Review

Review and prospect of $NiCo_2O_4$-based composite materials for supercapacitor electrodes

Yanmei Li[a], Xiao Han[a], Tingfeng Yi[a,c,*], Yanbing He[b,**], Xifei Li[d]

[a] School of Chemistry and Chemical Engineering, Anhui University of Technology, Maanshan 243002, Anhui, China
[b] Engineering Laboratory for the Next Generation Power and Energy Storage Batteries, Graduate School at Shenzhen, Tsinghua University, Shenzhen 518055, Guangdong, China
[c] School of Resources and Materials, Northeastern University at Qinhuangdao, Qinhuangdao 066004, Hebei, China
[d] Institute of Advanced Electrochemical Energy, Xi'an University of Technology, Xi'an 710048, Shaanxi, China

ARTICLE INFO

Article history:
Received 15 March 2018
Revised 18 April 2018
Accepted 15 May 2018
Available online 23 May 2018

Keywords:
$NiCo_2O_4$
Electrochemical performance
Synthesis
Morphology
Supercapacitors

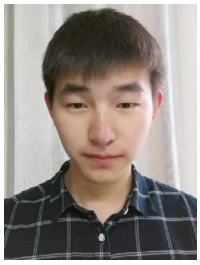
ABSTRACT

Supercapacitors known as typical electrochemical capacitors have been considered as one of the most promising candidates of energy storage systems owing to their advantages such as high-power density, long life span and lower production cost. The electrode materials play a crucial role on properties of supercapacitors. Hence, many researches have been focused on the development of novel electrode materials for high-performance supercapacitors. $NiCo_2O_4$ as supercapacitor electrode material has drawn more and more attentions in recent years due to its outstanding advantages, such as high theoretical capacity, low cost, natural abundance and easy of synthesis. However, the $NiCo_2O_4$ always suffer from severe capacity deterioration because of the low electrical conductivity and small surface area. Hence, it is necessary to systematically and comprehensively summarize the progress in understanding and modifying $NiCo_2O_4$-based materials from various aspects. In this review, the structure and synthesis method of $NiCo_2O_4$-based materials are discussed in detail. And then, the major goal of this review is to highlight new progress in using proposed strategies to improve the cycling stability and rate capacity of $NiCo_2O_4$-based materials, including synthesis, control of special morphologies and design of composite materials. Finally, an insight into the future research and development of $NiCo_2O_4$-based materials for supercapacitors is prospected.

© 2018 Science Press and Dalian Institute of Chemical Physics, Chinese Academy of Sciences. Published by Elsevier B.V. and Science Press. All rights reserved.



Yan-Mei Li received her Bachelor's degree from Anhui University of Technology in 2016. At present, she is pursuing her M. S. degree in Prof. Ting-Feng Yi's group at Anhui University of Technology. Her current research focuses on the application of functional materials in electrochemical supercapacitors.



Xiao Han received his Bachelor's degree from Anhui University of Technology in 2016. He is now a second year Master student in Prof. Ting-Feng Yi's group at Anhui University of Technology. His current research focuses on the application of transition metal oxides in lithium-ion batteries.



Ting-Feng Yi received his Ph.D. degree from Harbin Institute of Technology in 2007. He joined Anhui University of Technology as an assistant professor in 2007 and a full professor in 2011. He has now joined Northeastern University at Qinhuangdao as a full professor. He has published more than 95 papers in peer-reviewed journals as the first author or corresponding author, with 2600 citations (H-index = 28). His research interests include synthesis of electrochemical functional materials and their application in lithium-ion battery, supercapacitor and lead-acid battery. For detail please see his Research ID: http://www.researcherid.com/rid/F-4594-2012.

* Corresponding author at: School of Resources and Materials, Northeastern University at Qinhuangdao, Qinhuangdao 066004, Hebei, China.
** Corresponding author.
E-mail addresses: tfyihit@163.com (T. Yi), he.yanbing@sz.tsinghua.edu.cn (Y. He).

https://doi.org/10.1016/j.jechem.2018.05.010
2095-4956/© 2018 Science Press and Dalian Institute of Chemical Physics, Chinese Academy of Sciences. Published by Elsevier B.V. and Science Press. All rights reserved.



Yan-Bing He received his Ph.D. degree from the Department of Applied Chemistry, Tianjin University in 2010. He worked as a post-doctoral fellow at Graduate School at Shenzhen, Tsinghua University from 2010 to 2012 and a visiting scholar at Hong Kong University of Science and Technology from 2012 to 2013. He is currently an associate professor of Graduate School at Shenzhen, Tsinghua University. His research interests mainly focus on lithium ion power batteries and materials, solid state electrolyte and lithium metal anode.



Xifei Li is currently a full professor at Xi'an University of Technology and Tianjin Normal University, and he is an executive dean of Institute of Advanced Electrochemical Energy at Xi'an University of Technology. Dr. Li earned his bachelor degree in Electrochemistry Engineering from Harbin Institute of Technology, and he then completed his Master Degree and Ph.D. from General Research Institute for Nonferrous Metals of China and Xi'an Jiaotong University, respectively. He was awarded Ontario PDF and Mitacs Elevate Fellowship from 2009~2013 in Canada. Dr. Li's research group is currently working on design, synthesis, as well as performance improvement of the anodes and the cathodes with various structures for high performance lithium-ion batteries, lithium-sulfur batteries, sodium-ion batteries, and supercapacitors. Dr. Li has authored/co-authored more than 160 peer-reviewed research articles with more than 6000 citations and has fled over 15 patents and patent applications.

1. Introduction

The ever-increasing attention on the world energy crisis and environmental pollution has greatly boosted the development of electrochemical energy storage devices, such as rechargeable batteries, fuel cells and supercapacitors as energy storage systems for electric vehicles (EVs), hybrid electric vehicles (HEVs), plug-in hybrid electric vehicles (PHEVs), and smart grids [1–7]. For example, Ni/MH, lead acid batteries and lithium ion batteries as typical rechargeable batteries have been widely used as electrochemical energy storage devices and systems [8,9]. However, most of batteries suffer from low power delivery, and cannot satisfy the faster and higher-power energy requirements. In this situation, supercapacitors (SCs) were exploited to reserve and deliver energy with high rate capability, which has been well adapted to provide the electricity demand for electric vehicles, tramways, diesel-engine starting, wind turbines, computers, lasers, and cranes [10,11].

SCs, also known as ultracapacitors or electrochemical capacitors, can be fully charge-discharge only in a few seconds, leading to very higher charge/discharge power density (10 kW kg^{-1}) [12]. The Ragone plot as given in Fig. 1(a) exhibits the relationship of specific power density (W kg^{-1}) vs. specific energy density (Wh kg^{-1}) for miscellaneous electrical energy storage devices [13]. Obviously, the SCs are capable of perfectly fill the power-energy gap between conventional dielectric capacitors with great power output and batteries owning high energy density [14,15]. In short, SCs have the greatest potential in the field of energy storage devices [16].

According to the species of the electrode material and the mechanism of energy storage, SCs can originally be divided into three major categories [17–19], including electrical double-layer capacitors (EDLCs), pseudocapacitors (PCs) and hybrid capacitors in which the EDLC and PC coupling work together. In principle, the energy storage mechanism of EDLCs is on the basis of the electrostatic interaction between ions on the large specific surface area of active electrode materials and electrolytes. As shown in Fig. 1(b), a space charge layer in an electrode, a diffusive layer in an electrolyte and a tight Helmholtz layer are included in an EDLC, whose thickness is around 1 nm. A fast charge-discharge process occurring within seconds, and over 100,000 cycles can endure in EDLC systems. Carbon based materials are regarded as ideal electrode materials for EDLCs owing to their predominant characteristics such as controllable porous structures, flexible and stretchable, high conductivity, large surface area [20–22]. For instance, the activated carbon (AC), carbon aerogel, carbon fiber, carbon nanotube (CNT), porous carbon, and graphene manifest rapid charge storage performance [23]. Zhang et al. [24] discussed the advances and challenges of stretchable supercapacitors based on carbon materials and gave an overview of recent advances towards the development of carbon-based SSCs.

Pseudocapacitors mainly store charges by the rapid and reversible redox reactions on the surface of electrode materials, as shown in the right of Fig. 1(b). Typically, the transition metal oxides/hydroxides such as RuO_2, MnO_2, $Ni(OH)_2$, electrically conducting polymers (polyaniline (PANI), polypyrrole (PPy), etc.) and their composites could deliver high specific capacitance, but present poor cycle stability [25]. To improve their energy density, hybrid supercapacitors incorporating the favorable merits of EDLCs and pseudocapactiors have been developed, which sustain high power feature and meanwhile possess high energy density. According to the difference of two electrode materials adopted, hybrid supercapacitors could be generally divided into three classes including composite symmetric supercapacitors, battery-type supercapacitors and asymmetric supercapacitors (ASCs) [26]. Notably, ASCs consist of two different electrodes and are becoming a more popular kind of supercapacitors, which can achieve high energy density close to batteries and high-power density like supercapacitors (Fig. 1c) [27].

The performance of supercapacitors mainly includes five aspects, including work voltage, specific capacitance, specific energy (energy density), specific power (power density) and cycle life [28–31]. It is well reported that the energy storage performance of supercapacitors is directly related to the electrode materials. The preparation of electrode materials with stable performance and good electrical conductivity has been a hot research topic [32–35]. To date, grounded on the charge storage mechanism three kinds of electrode materials have been explored to fabricate the supercapacitors, including carbonaceous materials, high oxidation state transition metal oxides and conducting polymers [36–38].

With the desirable structural features and electrochemical activity, metal oxides have received more attention as supercapacitor electrodes. Meanwhile, metal oxide could overcome the poor capacity of carbon materials and avoid inferior cycle stability. In the past, pseudocapacitive materials of various transition metal oxides, such as MnO_2 [39], NiO [40], Co_3O_4 [41], V_2O_5 [42] and MoO_3 [43] are widely used because of their increasing specific capacitance, both energy and power densities. Recently, binary or ternary transition metal oxides have attracted extensive attention because of their outstanding electrochemical performance and electrical conductivity compared with the single-metal oxides. Binary metal oxides such as $NiCo_2O_4$, $MnCo_2O_4$, $CuCo_2O_4$, and $ZnCo_2O_4$ are of the origin of Co_3O_4. They have provided excellent performance in supercapacitors [44,45]. It is noteworthy that the electrical conductivity has the following order: $NiCo_2O_4 > NiO > Co_3O_4$, and many researchers have also verified that $NiCo_2O_4$ possessed a much lower resistance than nickel oxides and cobalt monoxides. The reaction mechanism for M_3O_4 (M = Co or Ni) during the charge storage process is as follows.

$$M_3O_4 + OH^- + H_2O \leftrightarrow 3MOOH + e^- \quad (1)$$

Benefiting from richer redox reaction from both nickel and cobalt ions than single component nickel oxides or cobalt oxides, the spinel nickel cobaltite ($NiCo_2O_4$) exhibits wonderful

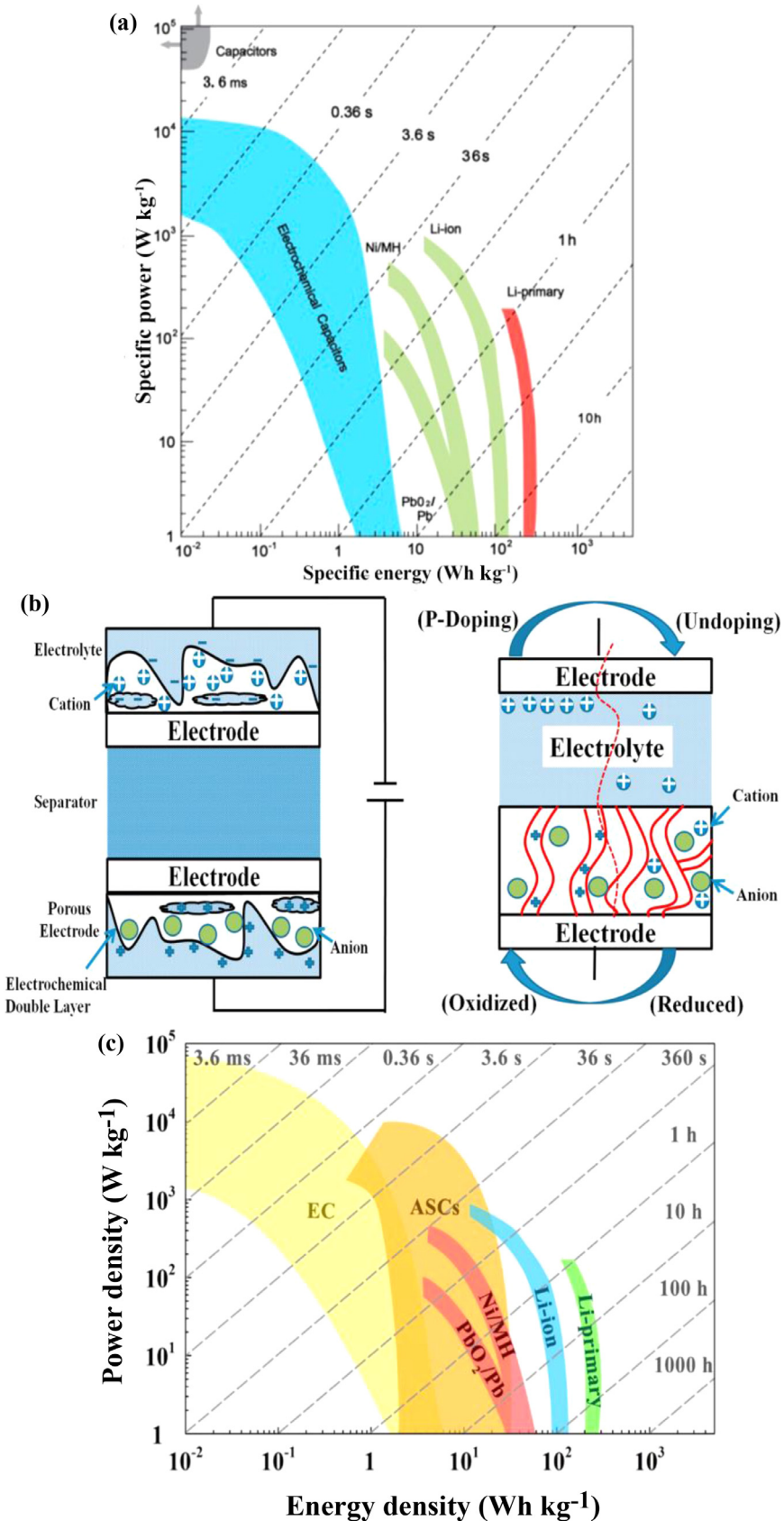


Fig. 1. (a) Ragone plot for various electrical energy storage devices [13]; (b) Aschematic diagram illustrating the operation principles of: (left) electric double layer capacitor (EDLC); (right) pseudo supercapacitor (PC) [13]; and (c) Ragone plot of ASCs with various typical electrochemical energy storage devices. Times given in the plot are the time constants of the devices, obtained by dividing the energy density by the power [27]. Reproduced from Refs. [14,27] with permission from Elsevier.

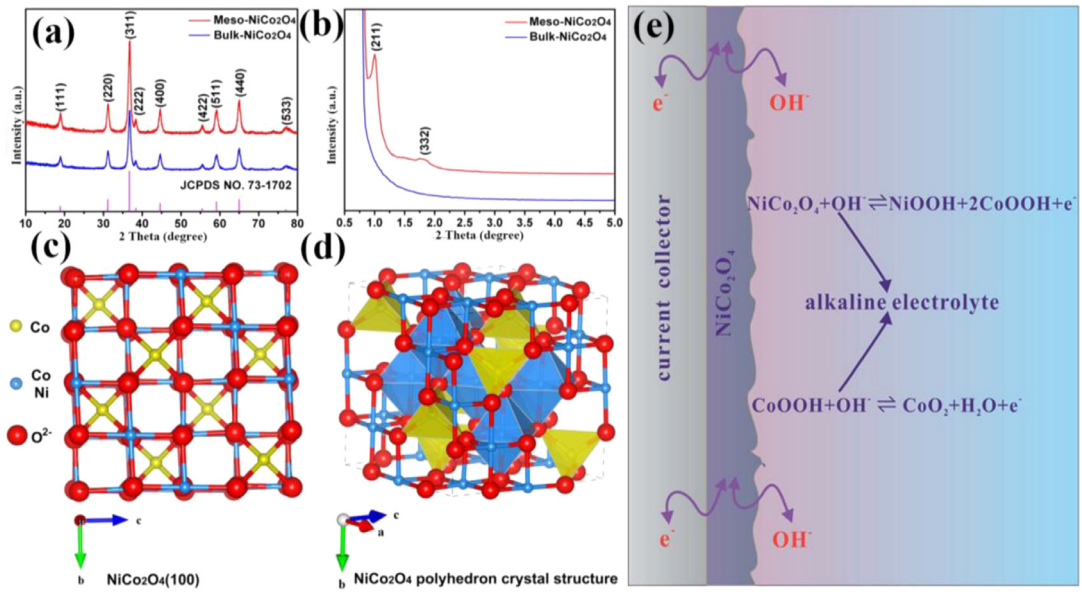


Fig. 2. (a) Wide-angle XRD, (b) low-angle XRD patterns of meso–$NiCo_2O_4$ nanospheres (red curve) and bulk-$NiCo_2O_4$ (blue curve), (c, d) crystal structure of $NiCo_2O_4$ (ICSD No. 24,211) [53] and (e) schematic of the charge storage mechanism of $NiCo_2O_4$ [57]. Reproduced from Ref. [53] with permission from American Chemical Society. Reproduced from Ref. [57] with permission from The Royal Society of Chemistry. (For interpretation of the references to color in this figure legend, the reader is referred to the web version of this article.)

electrochemical performance such as much better electrical conductivity and superior electrochemical activity [46,47]. More importantly, $NiCo_2O_4$ has some advantages such as low cost, natural abundance, environmental safety and low toxicity. Therefore, $NiCo_2O_4$ has become a more promising and flexible alternative electrode material for application in high-performance supercapacitors and has drawn more and more attention in recent years. Various $NiCo_2O_4$ materials with diverse morphologies, such as nanoparticles [48] and nanowires [49–51] have been reported. $NiCo_2O_4$ has multiple redox states and good electrical conductivity as a P-type semiconductor with a band gap of 2.1 eV [52]. Zhang et al. [53] prepared novel ordered meso–$NiCo_2O_4$ nanospheres and present the XRD pattern of meso–$NiCo_2O_4$ nanospheres and bulk-$NiCo_2O_4$. Obviously, there is no difference in wide-angle XRD patterns (Fig. 2a). However, in the low-angle XRD patterns (Fig. 2b), a sharp diffraction peak ($2\theta = 1°$) accompanied with a weak peak ($2\theta = 1.8°$) was founded in the meso–$NiCo_2O_4$ pattern, corresponding to the (211) and (332), which reflects 3D cubic $Ia\bar{3}d$ ordered mesoporous architecture. As shown in Fig. 2(c and d), the $NiCo_2O_4$ possesses a face-centered cubic (fcc) spinel structure with $Fd\bar{3}m$ symmetry with $a = 8.11$ Å and a strong (100) orientation, where all the nickel cations take up the octahedral interstices and the cobalt cations are occupied among the tetrahedral and octahedral gap [54]. In other cases, $NiCo_2O_4$ may be properly regarded as a nickel atom replacing one of the cobalt atoms in Co_3O_4. Obviously, the difference in physical properties and electrochemical performance between $NiCo_2O_4$ and Co_3O_4 is ascribed to the introduce of the nickel atom whose grain size is similar to that of cobalt atom that causes a little change in the crystal structure, in which the defects have some unexpected effects on electrochemical performance. An investigation of the cation valences in $NiCo_2O_4$ has been performed by means of X-ray absorption near edge structure (XANES), X-ray absorption fine structure (EXAFS) and ^{61}Ni Mössbauer spectroscopy. The oxidation state distributions of nickel cobaltite are uncertain, and the ionic configuration of $NiCo_2O_4$ is as the following formula: $Co_{1-x}^{2+}Co_x^{3+}[Co^{3+}Ni_x^{2+}Ni_{1-x}^{3+}]O_4$ ($0 \le x \le 1$). The cations before the square brackets are considered to be in the tetrahedral interstices and those within the square brackets are in the octahedral interstices [55,56]. As reported in some researches [57–59], in an alkaline solution, $NiCo_2O_4$ exhibits a potential window range of 0–0.55 V and its pseudo-capacitive behavior occurred in the alkaline electrolyte can be presented in the Fig. 2(e).

During the charge-discharge process, fast and reversible faradaic reactions occur on the surface of the electrode materials, where the valence state changes of Co^{3+}/Co^{4+}, as well as M^{2+} M^{-3+} (M = Co or Ni) exist. Interestingly, the specific capacitance of $NiCo_2O_4$ increased to some extent after several hundred cycles in some research, which was ascribed to their peculiar morphologies and the process of electrode activation [60,61]. However, the rate capability and electrochemical reversibility of $NiCo_2O_4$ electrodes are poor due to the nature of redox reaction. To resolve this problem, many effective strategies have been reported. Here, the structure and synthesis method of $NiCo_2O_4$-based materials are discussed in detail. And then, the major goal of this review is to highlight new progress in using proposed strategies to improve the cycling stability and rate capacity of $NiCo_2O_4$-based materials, including synthesis, control of special morphologies and design of composite materials. Finally, an insight into the future research and development of $NiCo_2O_4$-based materials for supercapacitors is prospected.

2. Preparation of $NiCo_2O_4$ materials

Advanced $NiCo_2O_4$ electrode material with unique nanostructure and high performance is expected by researcher and industry, while it is very difficult to find a universal and cost-effective routine to synthesize all types of $NiCo_2O_4$ nanomaterials by a one-pot approach [62–64]. In general, several methods have been used to prepare nanoscale $NiCo_2O_4$ oxide materials with variety of microstructures, including sol-gel, bio-template, electrodeposition process, electrospinning and hydrothermal. These synthesis methods are summarized and discussed in detail below.

2.1. Sol-gel method

Sol-gel method is a kind of facile and cheap method to produce ideal nanostructures with homogeneity, porosity and high purity. The sol-gel method generally covers four steps: the

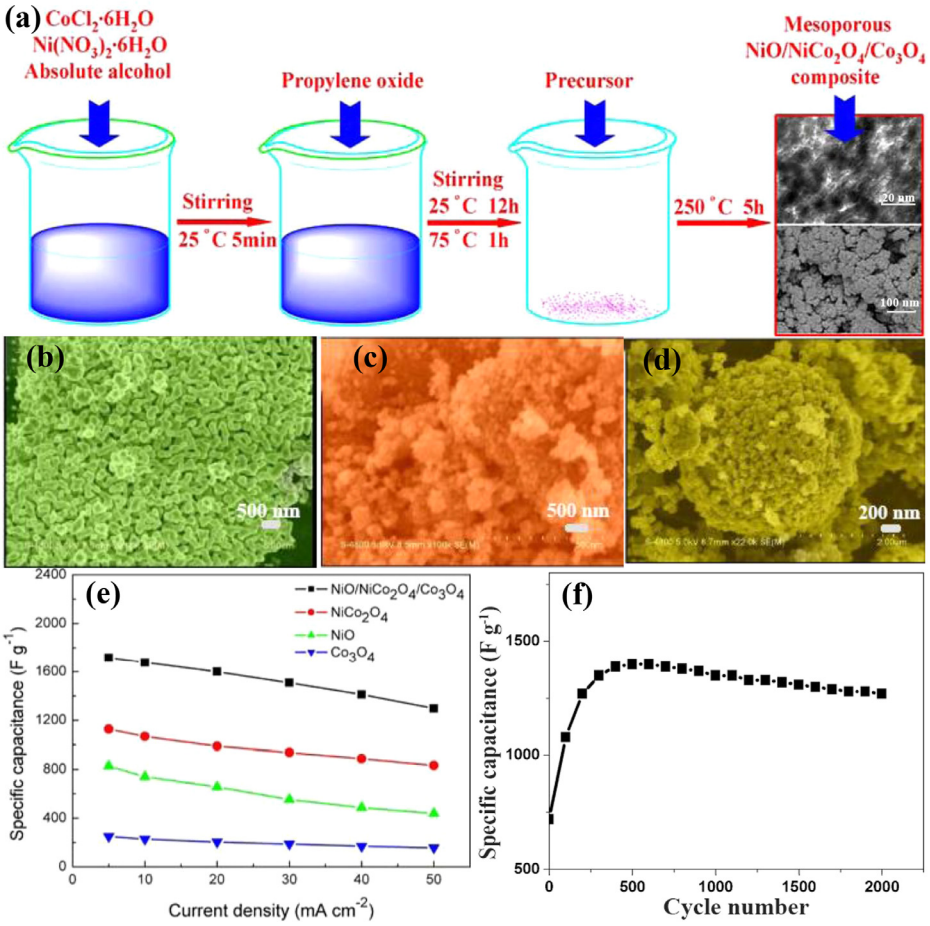
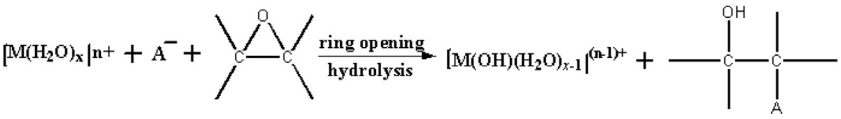


Fig. 3. (a) Synthesis procedure for mesoporous $NiO/NiCo_2O_4/Co_3O_4$ composite [69], FESEM images of as-obtained (b) sample (I), (c) sample (III) and (d) sample (II) [66], (e) specific capacitances of Co_3O_4, NiO, $NiCo_2O_4$, and NiO/ $NiCo_2O_4/Co_3O_4$ composite at a controlled current density [69] and (f) stability test in terms of specific capacitance for sample Ni–Co–O–200 [67]. Reproduced from Refs. [66,67] with permission from Wiley-VCH. Reproduced from Ref. [69] with permission from American Chemical Society.

fabrication of the precursor solutions, the formation of intermediate products as sol, the transformation from sol to gel and the calcination subsequently. In this process, solvents, reaction temperature, reaction time, surfactants have key influences to get the desired structures with extraordinary electrochemical performances [65]. For instance, in Wu's [66] work, $NiCo_2O_4$ coral-like porous crystals, nanoparticles and submicron-sized particles (Fig. 3b–d) have been methodically synthesized through a simple sol-gel method, employing H_2O (H_2O-DMF) as solvent and citric acid as the chelating ligand. The results indicate that submicron-sized $NiCo_2O_4$ particles show the prime capacitive performance with high specific capacitance and good cycle stability. Wei et al. [67] reported the synthesis of $NiCo_2O_4$ aerogels through an epoxide-driven sol–gel method for the first time, which exhibited high specific capacitance of 1400 F g^{-1} after additional 500 fully activate cycles of the Ni–Co–O–200 (see Fig. 3f), well reversibility and excellent cycle stability under a mass loading of 0.4 mg cm^{-2}. The majority of the pores sizes in the range of 2 to 5 nm were appropriate for supercapacitor applications. Liu and co-workers [68] fabricated $NiCo_2O_4$ crystals by a sol-gel method, which presents specific capacitance of 1128 F g^{-1} at a current density of 5 mA cm^{-2} and the specific capacitance retention is as high as 92.5% after 1000 cycles. In succession, mesoporous $NiO/NiCo_2O_4/Co_3O_4$ composite with high specific capacity (Fig. 3e) and high performance is fabricated by a sol-gel process and then calcined at 250 °C. The typical synthesize process of a sol-gel process is clarified in Fig. 3(a) and the mechanism of gelation can be described by the following reaction equation where M represents nickel or cobalt ions, and A^- represents Cl^- or NO_3^- ions [69].



(2)

Moreover, the submicron-sized $NiCo_2O_4$ particles with various morphologies and excellent properties were prepared using chelating ligand, different surfactants and organic-water binary solvent via a facile sol-gel process. Extensive researches are on-going through a sol–gel method to fabricate a better modality of $NiCo_2O_4$ so as to achieve a higher specific capacitance and excellent cycle stability. The sol–gel process has been confirmed to be a significant way to prepare $NiCo_2O_4$ electrode materials with low-cost and high electrochemical performance.

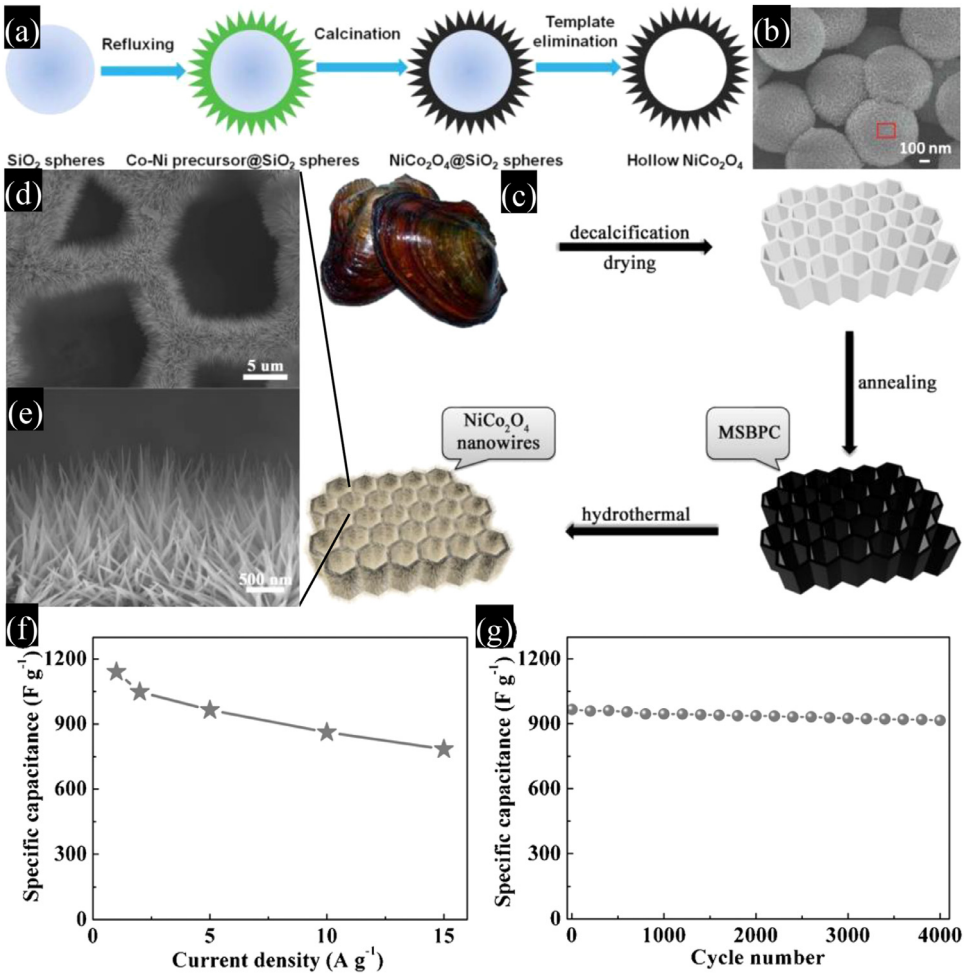


Fig. 4. (a) Schematic illustration of the formation of the mesoporous hollow $NiCo_2O_4$ sub-microspheres, (b) FESEM images for the hollow $NiCo_2O_4$ sub-microspheres [72], (c) preparation process of $NiCo_2O_4$/MSBPC composites, (d) SEM and (e) high-magnification SEM images of the $NiCo_2O_4$ nanowires [75], (f) specific capacitance at different current densities and (g) cycling performance of the $NiCo_2O_4$ electrode at a current density of 5 A g^{-1} [76]. Reproduced from Ref. [72] with permission from Royal Society of Chemistry. Reproduced from Refs. [75,76] with permission from Weilly-VCH.

2.2. Template method

Mesostructured transition metal oxides have dramatic advantages, such as high specific surface areas, controllable pore sizes and structures. These characteristics are significant for electrode materials because the particular morphologies can further accelerate the transportation of charge/ions in the electrode surface and electrolyte. Furthermore, the mesopores allow for the fast-redox reaction [70]. However, it is not easy to prepare mesoporous binary metal oxides due to the thermal instability. As the advancement of novel methods for the synthesis of mesoporous binary metal oxides, the template method is widely adopted combined with solvothermal/hydrothermal method for the fabrication of mesostructured binary metal oxides [71]. For instance, Yuan et al. [72] synthesized the uniform mesoporous hollow $NiCo_2O_4$ sub-microspheres using silica spheres as a hard-template (Fig. 4a). The obtained mesoporous hollow $NiCo_2O_4$ sub-microspheres self-assembled thoroughly by ultrathin nanosheets with a thickness of a few nanometers. They are very uniform in size and structurally robust by taking advantage of the in situ template removal (Fig. 4b). What's more, the hierarchical hollow $NiCo_2O_4$ sub-microspheres exhibit high specific capacitance of 678 F g^{-1} and excellent cycling stability of 87% (10 A g^{-1}) after 3500 successive cycles. In recent years, biological templates are abundant reserves, renewable, cheap, readily available and environmentally benign compared to artificial templates, such as graphene and carbon nanotubes (CNTs). There are many kinds of templates with inherently hierarchical and complex structures. Furthermore, even the same biology may also have different multilevel structures and morphologies. Therefore, bio-based carbon templates attract numerous researchers due to their natural highly ordered architecture with superior physicochemical properties, such as large surface area, great flexibility, and good mechanical strength. In addition, the bio-based carbon templates can be easily obtained without intricate chemical/physical conditions. Especially, it is propitious to electrolyte penetration and ion diffusion when they serve as the conductive substrate [73–76]. Thus, synthesis of simple and low-cost electrode materials with delicate framework derived from bio-template have obtained extensive exploration in recent years [77]. As shown in Fig. 4(c), Xiong et al. [78] employed mollusc shell as template and the $NiCo_2O_4$ nanowires grew directly on it by a facile hydrothermal strategy (Fig. 4d and e). Meanwhile, the shell based macroporous carbon material (MSBPC) with well-aligned microstructure and large number of pores honeycomb-like architecture was served as the conducting substrate. The as-synthesized $NiCo_2O_4$/MSBPC electrode presented large specific capacitance of 1696 F g^{-1} (1 A g^{-1}), super rate capability (even 421.8 F g^{-1} at 50 A g^{-1}), and excellent cycling stability (88% retention after 2000 cycles), revealing that the gained 3D carbon skeleton consisting of hexangular and highly ordered channels can efficiently

improve electrolyte penetration and rapid electron transfer. In addition, Shen et al. [79] exploited a novel and efficient self-template method for the preparation of uniform $NiCo_2O_4$ hollow spheres with a core-in-double-shell interior structure.

As exhibited in Fig. 4(f and g), the $NiCo_2O_4$ hollow spheres electrode possess excellent high-rate capability. At current densities of 1, 2, 5, 10, and 15 A g^{-1}, the electrode delivers high capacitance of 1141, 1048, 965, 862, and 784 F g^{-1}, respectively. Notably, the specific capacitance is about 914 F g^{-1} at 5 A g^{-1} after 4000 cycles with a high capacity retention of 94.7%. These works demonstrate that template-assisted method has specific advantage in preparing high-performance electrode materials [80]. Therefore, it is an effective way to prepare high-performance transition metal oxide electrode materials with high theoretical capacity for supercapacitors by using template-assisted method because of the advantages of the particular natural structure of template.

2.3. Electrospinning

Electrospinning is a comparatively complicated but multifunctional and cost-efficient way to fabricate well-established nanotubes and nanofibers with size in the range from several micrometers to tens of nanometers. During the preparation process, many important factors can influence the morphologies, size distributions, and diameters of the nanotubes and nanofibers, such as the concentrations of metal precursor, viscosity of precursor solution, type of polymer, and electrospinning parameters (applied voltage, working distance, and solution feed rate). The composite electrode materials with high capacitances and long cycle stability are achieved by the novel electrospinning method using the synergistic effect of different factors. For example, Li et al. [81] synthesized one-dimensional porous $NiCo_2O_4$ nanotubes (NCO–NTs) with porous architecture and hollow inside via electrospinning method. As shown in Fig. 5(b and c), the prepared nanofibers possess a mean diameter of about 89 nm and a length up to several micrometers (NCO–NFs). Because of their unique structure, the fabricated NCO–NT electrode displays a high specific capacitance of 1647 F g^{-1} at 1 A g^{-1}, excellent rate capability of 77.3% capacity retention at 25 A g^{-1}, and outstanding cycling stability of 93.6% after 3000 cycles (see Fig. 5e).

Furthermore, electrospinning has been regarded as a valid approach to prepare continuous fiber membranes as a binder-free carbonaceous template with micronsized or even nano-sized diameter, large specific surface area and excellent mechanical performances [82–84]. Owning to these prominent characteristics, electrospun carbon nanofiber (CNF) membranes are widely used as the electrode materials of supercapacitors [85–87]. In Addition, the electrospun CNF can remarkably enhance the conductivity of transition metal oxides or conductive polymers, which is favorable to maintain high specific capacitances of transition metal oxides even at larger current density [88,89]. The CNFs suffer a closed attachment for the $NiCo_2O_4$ particles, which could undertake good mechanical adhesion and excellent cycling stability. Lai et al. [90] developed a facile approach of growing δ-phase and γ-phase MnO_2 with distinctly different morphologies on highly conductive $NiCo_2O_4$-doped carbon nanofibers (NCCNFs) through the combination of electrospinning, solution co-deposition, and redox deposition methods to form core-sheath nanostructures with high performance. The formation process of NCCNF@MnO_2 nanosheet and nanorod is illustrated in Fig. 5(a). The relationship between scan rate and the specific capacitance shows an excellent rate stability (Fig. 5d). For the NCCNF@MnO_2 NR hybrid membrane, the specific capacitance reaches 146 F g^{-1} (based on whole materials) even at a scan rate of 100 mV s^{-1}.

2.4. Electrodeposition

The electrodeposition process occurs in the electrolysis of related plating solutions where micron- or submicron-size molecules are dissolved, and large amounts of particles according to the stoichiometric ratio are embedded in the electrochemically produced composite with special performance [91]. In principle, the electrodeposition process can be classified into three steps, including preparation of a precursor solution, co-electrodeposition of precursor, and thermal decomposition transformation. Facile electrodeposition synthesis methods and subsequent thermal treatment have been diffusely adopted to prepare 2D metal oxide nanosheets. Recently, some conductive substrates also have been served as current collector to further improve electrochemical performance of the electrode materials, such as single-walled carbon nanotube, carbon fabric and nickel foam. For instance, the carbon fabric (CF) is an ideal conductive substrate for directly growing active material because of the excellent electronic conductibility, good flexibility, advanced mechanical strength and inexpensive [92]. Therefore, some researchers have used CF as conductive substrate to support active material. For example, An et al. [93] reported the facile co-electrodeposition of $NiCo_2O_4$ radially on carbon cloth with good electrochemical properties. The schematic illustration of the synthesis of honeycomb-shaped $NiCo_2O_4$/CC (HSNC) is displayed in Fig. 6(a). With deposition time goes on 120 s, $NiCo_2O_4$ nanoparticles would voluntarily be attached to the generated sheets because of the minimization of facet free energy (Fig. 6b) [94].

Wu et al. [95] prepared the homogeneous thin $NiCo_2O_4$ nanosheets onto nitrogen-doped carbon nanotubes (N–CNTs) through a facile electrochemical deposition method. The electrodeposited cubical- and hexagonal-shaped $NiCo_2O_4$ particles with some micro porous space were shown in Fig. 6(c). The electrochemical performances were displayed in Fig. 6(d and e). The SCs are 2658, 2200, 2170, 2000, 1866 F g^{-1} at different current densities of 2, 5, 10, 15, and 20 A g^{-1}, respectively. The result reveals about 70% of the initial SC is remained even at a high current density of 20 A g^{-1}, indicating that the obtained $NiCo_2O_4$/CF composites possess extraordinary rate performance. Moreover, the SC of the electrode decays approximately 20% after 3000 cycles, indicating high electrochemical stability for long cycle life. Besides, the electrodeposition is also one of the most common methods in preparing various nanomaterials composites. Several composite electrodes such as Co_3O_4@$NiCo_2O_4$ [96] and $Ni(OH)_2$@$NiCo_2O_4$ [97], have also been synthesized by the electrodeposition route. However, the precise relationship between the composite structure and electrochemical properties has not been verified yet.

2.5. Hydrothermal method

From the discussion mentioned above, it can be found that the synthesis method plays a key role on the preparation of nanomaterials and improvement of pseudocapacitive performance. In recent years, hydrothermal reaction also has been considered as a promising approach to synthesize nanostructures due to its environmentally benign, and good controllability of reaction condition and controlled production of various nanostructures at high pressure and moderate temperature including nanowires, nanosheets, nanoflowers and so on [98]. The $NiCo_2O_4$ precursors were also prepared using hydrothermal reaction by a mixture of related metal salts reagent, and then were heated in a sealed Teflon-lined stainless-steel autoclave. As a wide-used method of preparing $NiCo_2O_4$, it is necessary to synthesis highly monodispersed nanoparticles with controllable size and unique morphology [99]. In addition, many groups have made great efforts to optimize the reaction conditions to form special morphologies with enhanced electrochemical performance of $NiCo_2O_4$ electrodes

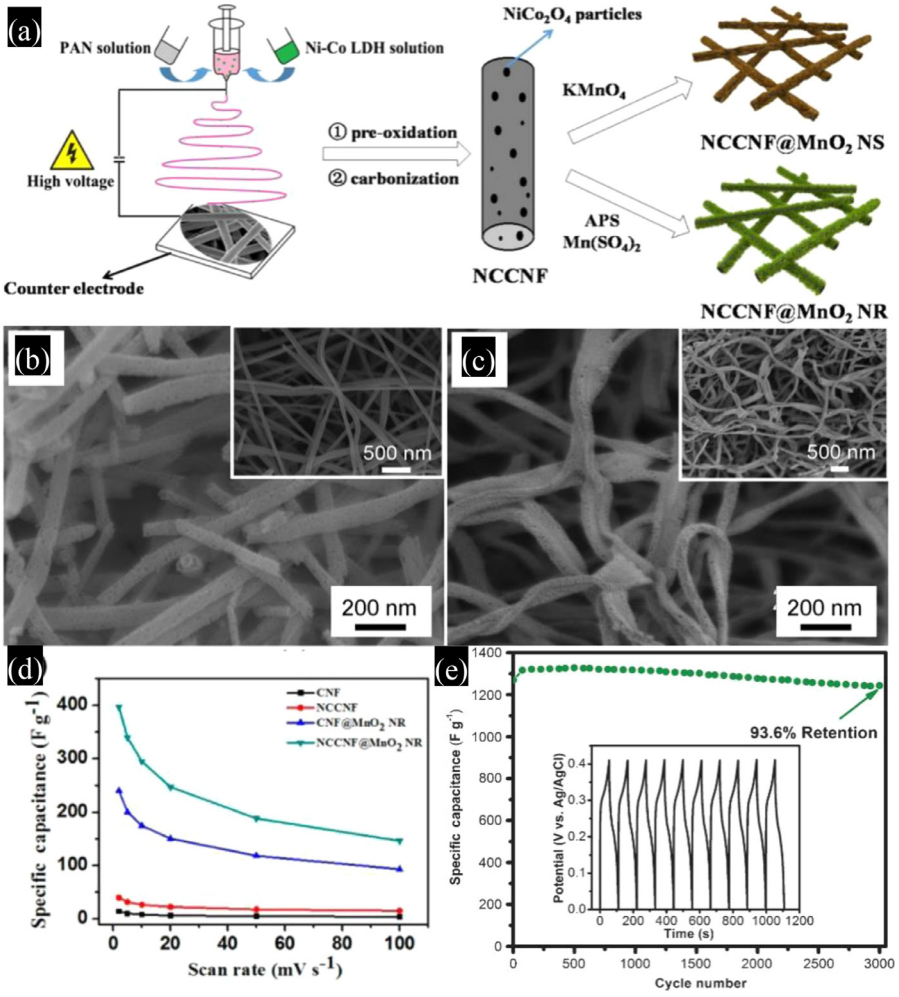


Fig. 5. (a) Schematic illustration for the preparation of NCCNF@MnO_2 NS and NR hybrid membranes [90], SEM images at high and low (inset) magnifications for (b) NCONFs and (c) NCO–NBs [81], (d) rate stability of bare CNF, NCCNF, CNF@MnO_2 nanorod, and NCCNF@MnO_2 nanorod membranes at different scan rates [90] and (e) cycling stability of NCO–NTs at a current density of 10 A g^{-1}. The inset shows the first ten charge/discharge curves of NCO–NT [81]. Reproduced from Ref. [81] with permission from Weilly-VCH. Reproduced from Ref. [90] with permission from American Chemical Society.

[100–104]. Wang et al. [105] successfully prepared 3D hierarchical $NiCo_2O_4$ with tremella-like (T-$NiCo_2O_4$), flower-like (F-$NiCo_2O_4$), urchin-like (U-$NiCo_2O_4$) and pine-needle-like (P-$NiCo_2O_4$) structures through a facile hydrothermal method. As shown in Fig. 7(a), the morphologies of $NiCo_2O_4$ can be controlled by varying the categories of alkali sources and adding NH_4F, and the electrochemical performance can be affected. The important roles of alkali source and NH_4F in fabrication of these nanostructures have been researched. The as-prepared four $NiCo_2O_4$ electrode materials were designed to continuous galvanostatic charge–discharge (GCD) measurements at a large current density (10 A g^{-1}) for 1000 cycles. As displayed in Fig. 7(b), there was no obvious capacitance decline observed for all the four materials, revealing their excellent cycling ability.

Very recently, some surfactants, such as polyvinylpyrrolidone (PVP), polyvinyl alcohol (PVA) and hexadecyltrimethylammoniumbromide (CTAB) [106–108], have also been used as the structure-directing agent to prepare electrode materials with unique morphologies and high electrochemical performance. However, the use of surfactants and growth-directing agents usually reduces the charge transfer in the target products and thus weakens the electrode material performance. Fortunately, a unique laser ablation in liquid (LAL) method could conduce to prepare high activity precursors by prefabricating ternary oxide nanocrystals (TONs) with a clean surface, which can acquire enhanced charge transport in the electrochemical energy storage devices [109]. It is necessary to develop other feasible technology to improve the performance of electrode materials, such as ion-doping and transition metal oxides modification. For example, a porous vanadium doped-zinc–nickel–cobalt ternary oxide (VZnNiCo) nanostructure has been used to high performance flexible supercapacitor [3]. Moreover, dandelion-like Fe-doped $NiCo_2O_4$ microspheres@nanomeshes (Fe-NCO-M@N-1 h) prepared by a facile hydrothermal method shows high specific capacitance, excellent rate performance and remarkable cyclic stability [5]. Successively, self-supported 3D ultrathin porous quaternary Zn-Ni-Al-Co oxide nanosheets with hierarchical, porous structures, are regarded as auspicious electrodes for high-performance hybrid supercapacitors [7]. In summary, various nanostructured types $NiCo_2O_4$-based materials with 1D, 2D or 3D morphology can be obtained by using facile hydrothermal method.

2.6. Summary of preparation methods

In short, this section suggests five means to synthesize $NiCo_2O_4$-based electrode materials, including sol-gel, bio-template, electrodeposition, electrospinning and hydrothermal methods. Each method has advantages and drawbacks. The sol-gel method is inclined to prepare 0 D structures such as nanoparticles with homogeneity, porosity and high purity. The template method, especial biological templates with abundant reserves, renewable and

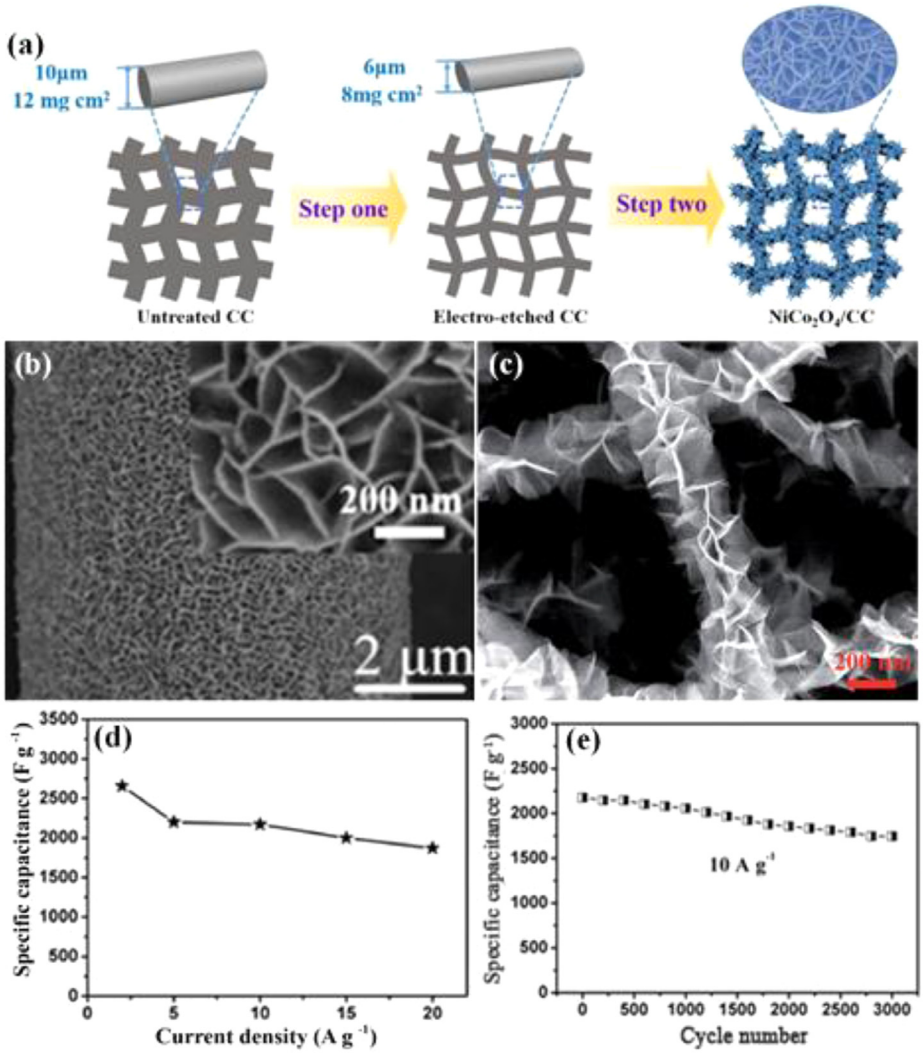


Fig. 6. (a) Schematic illustration of electrodeposition process for forming the $NiCo_2O_4$ samples, (b) FESEM images of samples for 120 s [93], (c) high-magnification SEM image of the N–CNT/$NiCo_2O_4$ nanosheets [95], (d) corresponding specific capacitance at different current densities and (e) cycling performance at a current density of 10 A g^{-1} [92]. Reproduced from Refs. [92,93] with permission from American Chemical Society. Reproduced from Ref. [95] with permission from Springer.

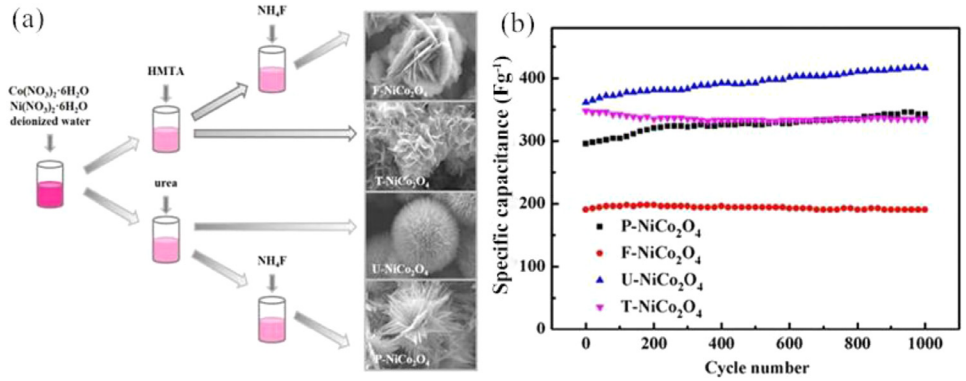


Fig. 7. (a) Schematic diagram illustrating the hydrothermal process of fabricating F-$NiCo_2O_4$, T-$NiCo_2O_4$, U-$NiCo_2O_4$ and P-$NiCo_2O_4$ and (b) cycling performance of the different $NiCo_2O_4$ electrodes at high current density of 10 A g^{-1} [104]. Reproduced from Ref. [104] with permission from The Royal Society of Chemistry.

environmentally benign, can be fabricated highly ordered architecture electrode materials with special shapes. Electrospinning is usually used in preparing one-dimensional (1D) fiber with a diameter in the range from several micrometers to tens of nanometers. Electrodeposition process possesses some significant advantages to deposit $NiCo_2O_4$ onto conductive substrates and to combine $NiCo_2O_4$ with some other high-performance materials with favorable synergistic effect, which can be controlled by changing concentration and pH value of solution and applying overpotential or current density. By comparison, the hydrothermal process is a direct and effective way to synthesize one-dimensional (1D), two-dimensional (2D) and three-dimensional

(3D) nanostructured $NiCo_2O_4$-based materials with unique architectures and superior electrochemical performances by adjusting temperature parameters, the kinds and concentration of surfactants. Many researchers have explored to prepare different morphologies of $NiCo_2O_4$ including 1D, 2D and 3D nanostructures. Compared with 1D and 2D nanostructures, 3D nanostructure has more advantages in energy storage materials. 3D structural morphology not only forms the desired hierarchical porous continuous channels for electrolyte ions by serving as an ion buffering reservoir, but also has higher electrical conductivity and excellent structural mechanical stability, which can alleviate the volume expansion effect during charge/discharge process.

3. Nanostructured $NiCo_2O_4$ electrodes with different morphologies

3.1. Pristine $NiCo_2O_4$

As we know, the physical and chemical properties of materials are dramatically changed when the particle size is decreased to the nanoscale. Nanomaterials are expected to bring important improvements for energy storage devices [110]. The cross-linked network in nanostructures includes nanowires, nanoneedles, nanosheets, nanoarrays and nanoflowers. 1D nanostructures can provide direct current pathways, shorten the ion diffusion length, reduce the charge–discharge time, increase the electrolyte–electrode contact area, limit mechanical degradation, and accommodate volume expansion [111]. Due to the inherently high specific surface area and distinctive electronic properties of ultrathin sheets, 2D nanomaterials are popular for energy storage and conversion system. Besides the above advantages, 2D materials also show other special properties such as flexibility, high packing densities, mechanical stability and transparency, which prompt them fit for the development of flexible and wearable electrochemical capacitors [112]. Compared with 1D and 2D nanostructures, the complex 3D structures contributed by 1D nanostructures possess unique properties because they incorporated the advantages of all related nanoscale building-blocks [113]. In addition, homogeneous hierarchical 3D nanostructures assembled from nanotubes, nanoflakes, nanowires, or nanorods with several levels of structure, also have exhibited super capacitive property because of the large SSA (specific surface area) and high density of defects arising from nanoscale building blocks and have numerous promising applications in many professional fields such as chemical sensors [114], catalysis [115], batteries [116,117], electrochromic devices [118] and supercapacitors. Generally, it is important for SCs to achieve large specific surface area and fitting pore size distribution suitable for decreasing the consumption of electrolyte by regulating porous structure of electrode materials. For example, Liang et al. [119] successfully prepared $NiCo_2O_4$ nanosheets@halloysite nanotubes (Fig. 8a and b) by a facile coprecipitation route followed by a thermal annealing treatment. The specific capacitance can reach 1728 F g^{-1} at the end of 8600 cycles at a current density of 10 A g^{-1} and a capacity loss of 5.26%. As shown in Fig. 8(c and d), novel hierarchical $NiCo_2O_4$ nanosheets@hollow microrod arrays (NSs@HMRAs) were prepared by a simple and environment-friendly template-assisted electrodeposition followed through thermal annealing [120]. Owing to their unique nanostructures, the $NiCo_2O_4$ NSs@HMRAs showed a high specific capacitance (C_{sp}) (678 F g^{-1} at 6 A g^{-1}) and excellent cycle stability (C_{sp} retention of 96.06% after 1500 cycles). Additionally, a kind of $NiCo_2O_4$ pseudocapacitive materials with an urchin-like hollow micro-sphere structure (UHMS) ware designed and fabricated (Fig. 8e and f). The as-synthesized $NiCo_2O_4$ UHMS sample exhibited an improved specific capacitance of about 942.2 F g^{-1} at a current density of 0.5 A g^{-1} and excellent rate capability [121].

Traditional dielectric capacitors and batteries usually include a sandwiched separator between two electrodes in an ionic liquid electrolyte. The electrodes usually include binders, and the binders often affect the performance of the electrodes, and then affect the practical engineering applications of the device, such as wearable flexible SC. Consequently, it is necessary to develop a new technique, by which nanostructured electrode materials can be in-situ formed on the surface of conductive substrates, especially on 3D porous substrates. This is a binder/additive-free electrode for electrochemical capacitors. These binder/additive-free electrodes avoid the “non-activated surface” in traditional slurry-derived electrodes. In addition, it also brings high charge-discharge rate capability due to the shortened transport path length for both electrons and ions and is beneficial to the charge transfer. And it also provides effective interface contact between current collector and active materials, resulting in highly enhanced electrochemical performance. Compared with powdery nanomaterials, self-supported nanoelectrodes offer particular benefits over the slurry-casting electrodes such as enhanced utilization of electroactive materials and improved charge/ion transport efficiency. One of the most common ways of getting nanoelectrodes is to directly fabricate electroactive materials into the forms of free-standing either 1D nanoarrays, 2D nanoarrays, or 3D nanoporous architectures on conductive substrates [122–124]. Usually, these nanoelectrodes are called as self-supported uniform nanoelectrodes (Fig. 9), because the nanoelectrodes are nanoarrays of only single electroactive material. Additionally, there are also self-supported heterogenous nanoelectrodes for supercapacitors that mean the nanoarrays include either electroactive substances with nanostructured current collectors/supporters or more than one type of electroactive substances in single nanoelectrodes (Fig. 9). Generally, self-supported heterogeneous nanoelectrodes with a core-shell structure consists of a shell of active materials uniformly deposited on a core of independent nanostructured current collectors or another kind of active materials that are directly grown on a conductive substrate [125].

Chen and co-workers directly grew $NiCo_2O_4$ nanosheets on flexible carbon fabric through an electrochemical deposition method and the specific capacitances (SCs) of composites are as high as 2658 F g^{-1} (2 A g^{-1}) [126]. Zou et al. reported a 3D microsphere composed of radial chain-like $NiCo_2O_4$ nanowires with a SC of 1284 F g^{-1} (2 A g^{-1}) by a facile hydrothermal route and thermal decomposition [127]. To improve the electrochemical performance of $NiCo_2O_4$, the nanostructured $NiCo_2O_4$ (such as nanowires, nanosheets, nanotubes) with high specific capacitance and excellent rate capabilities can be used as substrates for $NiCo_2O_4$-based composite. Other compounds directly grow on these $NiCo_2O_4$ substrates, and can form $NiCo_2O_4$-based composite, which has more excellent electrochemical performance than pristine nanostructured $NiCo_2O_4$.

3.2. $NiCo_2O_4$-based composite materials

Unfortunately, single $NiCo_2O_4$ often exhibits limited kinetics during the redox reaction because of the low electrical conductivity or easily agglomerate in substrates, leading to the poor capacitance, inferior cycling stability and bad rate performance. In addition, the active material near the bottom is difficult to participate in the electrochemical charge storage process because of the limited electrolyte diffusion in supercapacitor electrodes, which results in an unsatisfactory ASC (areal specific capacitance). An efficient solution is to design the nanocomposite architectures. Currently, it was discovered that $NiCo_2O_4$ with well-organized nanostructures, such as nanowires, nanosheets, nanorods and nanotubes, can combine with other kinds of materials like car-

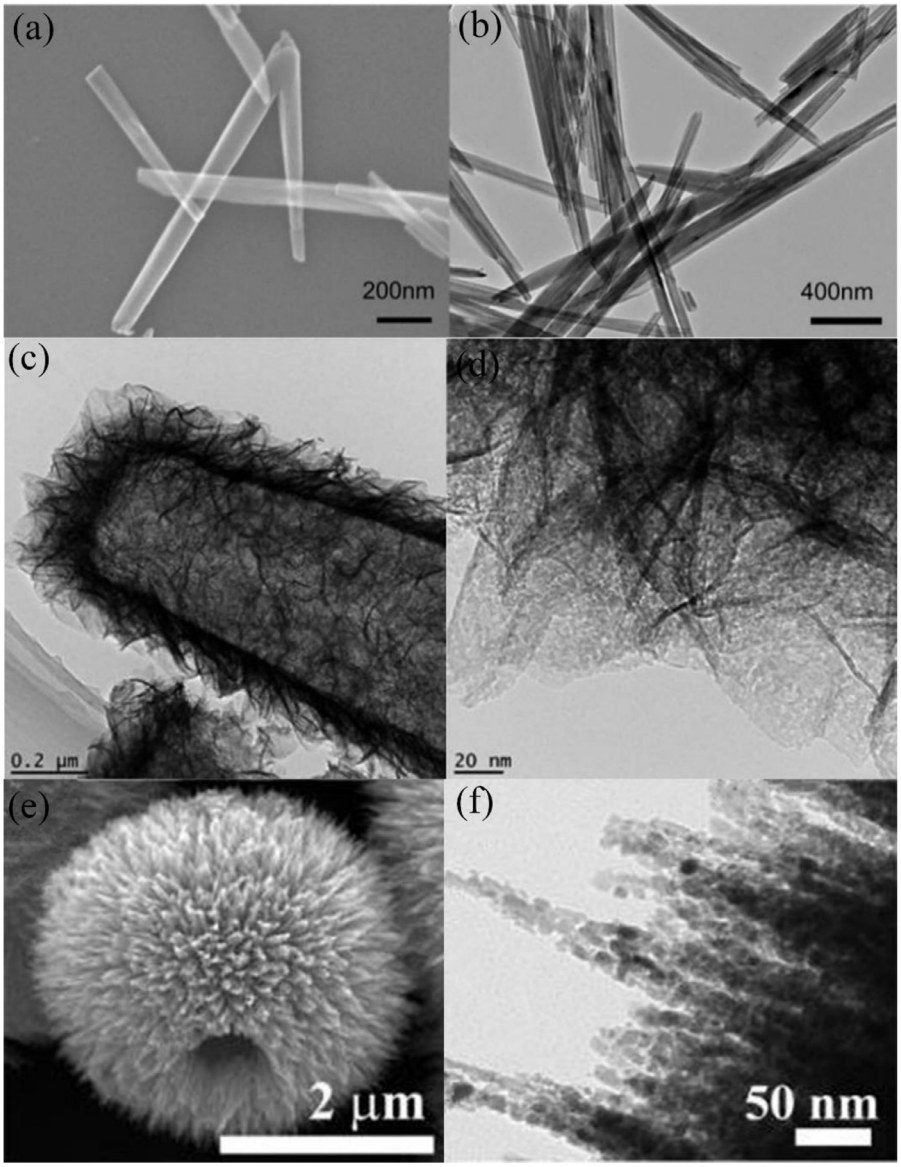


Fig. 8. (a) SEM and (b) TEM image of the halloysite nanotubes [120], (c) and (d) TEM images of $NiCo_2O_4$ NS@HMRAs [119], (e) SEM and (f) TEM images of the final $NiCo_2O_4$ UHMS [121]. Reproduced from Refs. [119,121] with permission from The Royal Society of Chemistry. Reproduced from Ref. [120] with permission from American Chemical Society.

bon, metal oxides/hydroxide, conducting polymers, metal-organic frameworks (MOFs) and covalent-organic frameworks (COFs) to improve the performance of $NiCo_2O_4$. The resulting functional hierarchical nanostructures or "core-shell" configurations contribute to a more high-level of electrochemical performance [128]. The electrode material design with "core" and "shell" structure can achieve a desired synergistic effect [129]. This effective approach to fabricate hybrid materials composites not only possess the advantages of all the constituents, but also overcome the disadvantages of individual components. Hence, construction of different structures with the combination of two different materials has been proved to be a promising strategy to boost the electrochemical performance of metal oxides [130].

3.2.1. $NiCo_2O_4$-metal oxide composites

Recently developed hierarchical nanostructures obtained by metal oxide directly grown on an active material (current collector) show remarkable merits [131]. Generally, they can enlarge the contact area between active materials and the electrolyte, increase the porosity, and provide more active materials in a given unit area without any auxiliary components, resulting in higher electrochemical properties [132,133]. Recently, significant efforts have been taken to controllable synthesis of perfected core/shell nanowire heterostructures by combination of two types of materials, which show improved electrochemical performances. For example, Chen et al. [134] obtained a heterostructures composite by coating a $NiWO_4$ nanosheets on self-supported $NiCo_2O_4$ nanowire arrays, which presents a high enhancement of specific capacitance of 1384 F g^{-1} at a current density of 1 A g^{-1} and superior cycling stability (87.6% retention over 6000 cycles at a current density of 5 A g^{-1}). However, the pristine $NiCo_2O_4$ electrode only shows a specific capacitance of 865.3 F g^{-1} at the corresponding current density. $NiCo_2O_4$ has relatively high electrical conductivity but low capacitance. Conversely, $MnMoO_4$ possesses high capacitance but inferior electrical conductivity. The combination between $MnMoO_4$ and $NiCo_2O_4$ can reach their full advantages of both materials. For example, Wang and co-workers [135] synthesized the $NiCo_2O_4$@$CoMoO_4$ nanowire/nanoplate arrays, and the capacitance could reach 14.67 F cm^{-2} at the current density of 10 mA cm^{-2}, with a capacitance decrease of 25.9% after 1000 cy-

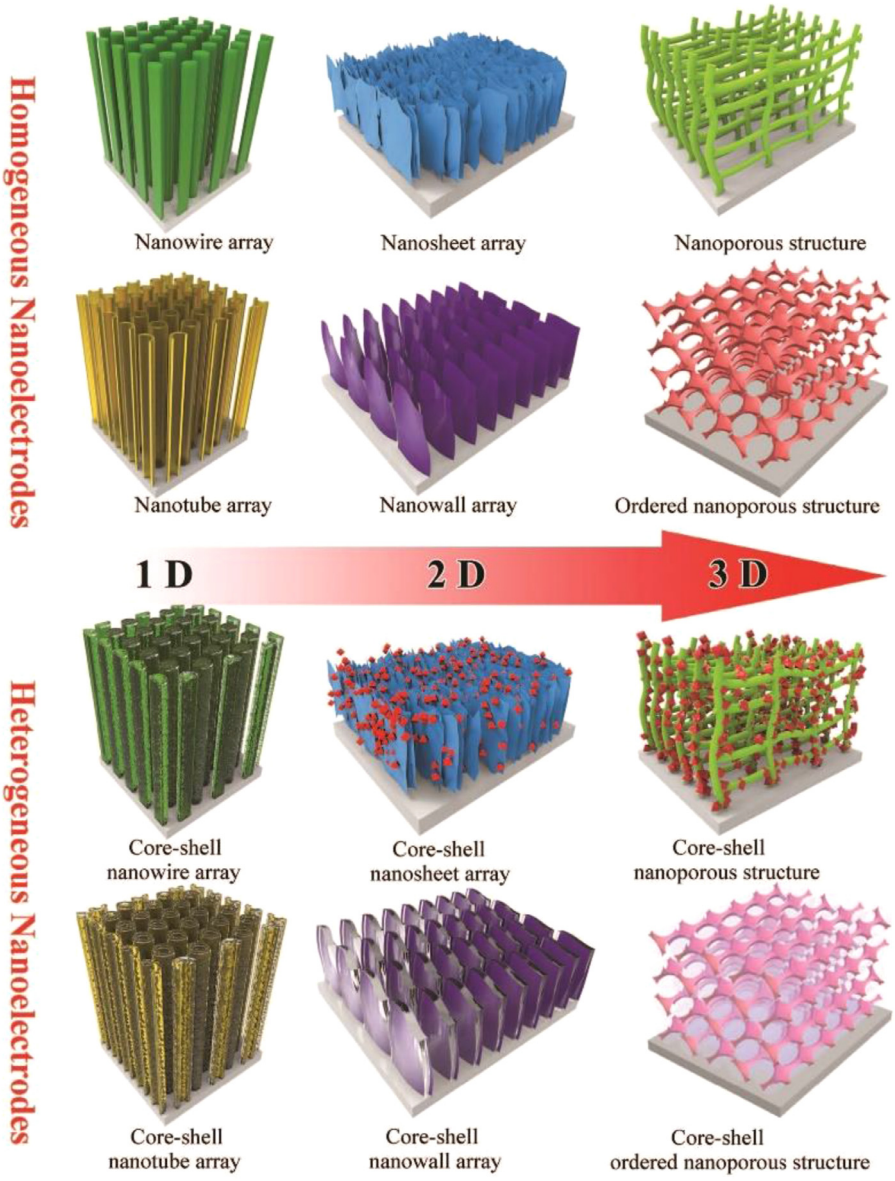


Fig. 9. Schematically illustrating the typical geometries of self-supported homogeneous and heterogeneous nanoelectrodes for supercapacitors [125]. Reproduced from Ref. [125] with permission from Wiley-VCH.

cles. Besides, many groups [136–138] grew $MnMoO_4$ nanowires onto the backbone material $NiCo_2O_4$ nanowire arrays in the aqueous solution system to prepare hierarchical 3D heterostructured $NiCo_2O_4$@$MnMoO_4$ nanocolumn arrays (NCAs) on Ni foam. The crystal growth method during the complicated nanoarchitecture process was "self-assembly" and "oriented attachment". As shown in Fig. 10(a, b), firstly, the $NiCo_2O_4$ nanowire array was directly grown on nickel foam. In the hydrothermal process, the as-prepared $NiCo_2O_4$ nanowires on nickel foam acted as templates and then $MnMoO_4$ nanosheets were uniformly wrapped in the surface of the $NiCo_2O_4$ nanowires, forming $NiCo_2O_4$@$MnMoO_4$ composite nanocolumn arrays. The core-shell structure could supply short electron/ion transfer path and significantly improve the electrochemical property.

The as-synthesized $NiCo_2O_4$@$MnMoO_4$ and $NiCo_2O_4$@$NiMoO_4$ core–shell nanoflowers are uniformly attached on the substrate, the $MnMoO_4$ and $NiMoO_4$ nanoflowers are very thin, which can be observed in the magnified images of Fig. 10(c–e). $NiCo_2O_4$ nanowire is fully wrapped by a great amount of $MnMoO_4$ nanosheets. The electrochemical test reveals that the obtained hybrid $NiCo_2O_4$@$MnMoO_4$ electrode exhibits superior pseudocapacitor performances with high capacitance of 1705.3 F g^{-1} at 5 mA cm^{-2}, and retaining 92.6% after 5000 cycles. However, the bare $NiCo_2O_4$ electrode only shows a capacitance of 839.1 F g^{-1} and a retention of 90.9% at the corresponding current density after 5000 cycles. In addition, the charge-transfer resistance (R_{ct}) of $NiCo_2O_4$ and $NiCo_2O_4$@$MnMoO_4$ electrodes before and after cycles is investigated. It can be observed that the R_{ct} increased with the increase of cycling number with 0.12 Ω at 50 cycles, 0.17 Ω at 2500 cycles, and 0.56 Ω at 5000 cycles, respectively. There is a conductance deterioration during cycling. However, the R_{ct} is still satisfactory, indicating that there is no great change of R_{ct} for both electrodes even after 5000 cycles. Notably, the $NiCo_2O_4$@$MnMoO_4$ shows higher ASC (area specific capacitance) than pristine $NiCo_2O_4$. As shown in Fig. 10(f), the ASCs of $NiCo_2O_4$@$MnMoO_4$ are 1.91, 1.78, 1.62, 1.39, and 1.19 F cm^{-2} at current densities of 1, 2, 5, 10, and 20 mA cm^{-2}, respectively. However, the corresponding ASCs of pristine $NiCo_2O_4$ are only 0.93, 0.84, 0.73, 0.62, and 0.52 F cm^{-2}, respectively. Obviously, $NiCo_2O_4$@$MnMoO_4$ has much higher ASCs

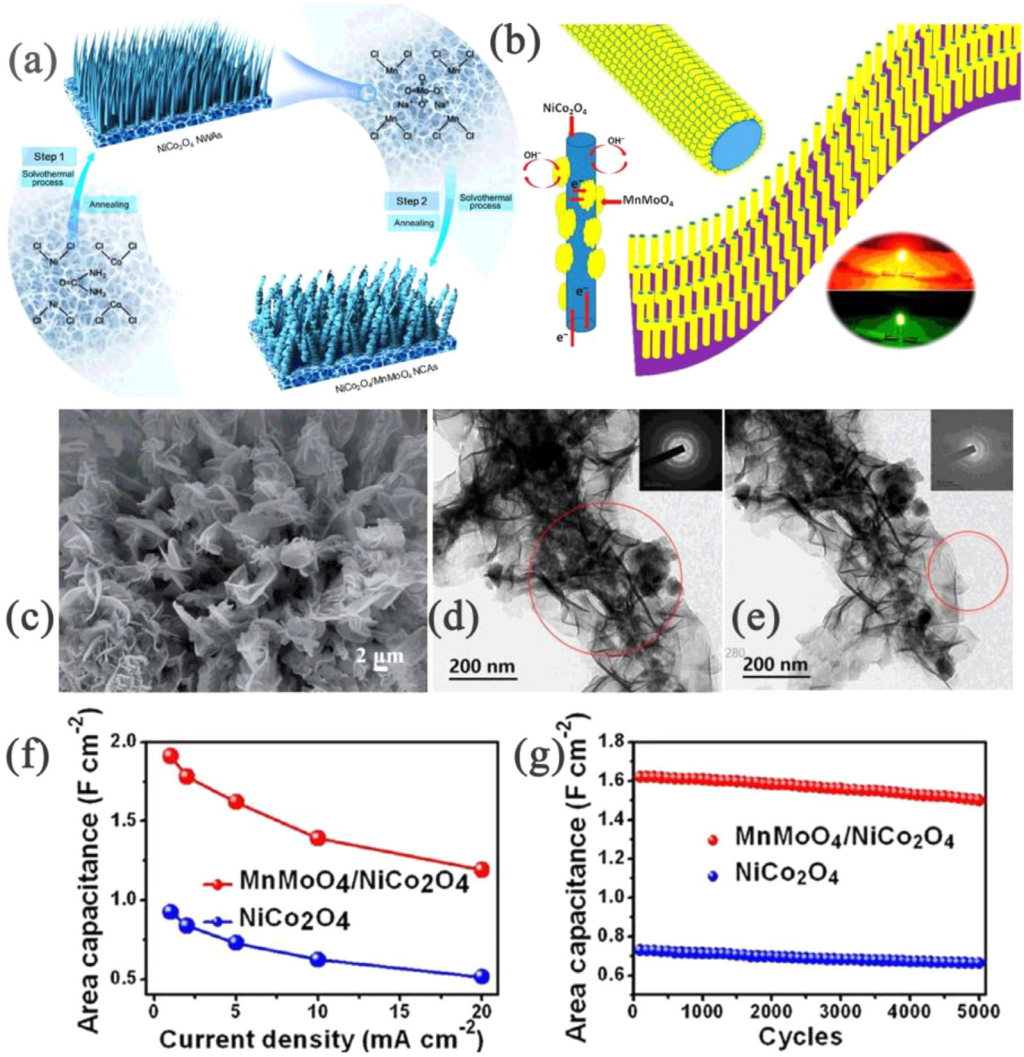


Fig. 10. (a) Schematic fabrication process of $NiCo_2O_4$@$MnMoO_4$ hybrid NCAs on Ni foam [136], (b) schematic mechanism model of $NiCo_2O_4$@$MnMoO_4$ core – shell nanoarrays [138], (c) typical SEM images of the $NiCo_2O_4$@$NiMoO_4$ nanoflowers (NFRs) on Ni foam [137], (d) TEM image of $NiCo_2O_4$@$MnMoO_4$, the inset image shows the SAED of $NiCo_2O_4$@$MnMoO_4$ corresponding to the area where both core and shell are characterized as the red circle assign [138], (e) TEM image of $NiCo_2O_4$@$MnMoO_4$ (the inset image shows the SAED of $NiCo_2O_4$@$MnMoO_4$ corresponding to the area where only shell is characterized as the red circle assign [138]), (f) ASC and (g) cycling performance of $NiCo_2O_4$ and $NiCo_2O_4$@$MnMoO_4$ electrodes at various current densities [136]. Reproduced from Refs. [136,138] with permission from American Chemical Society. Reproduced from Refs. [137] with permission from The Royal Society of Chemistry.

than the pristine $NiCo_2O_4$ at each current density. In addition, the cycling stability of the $NiCo_2O_4$@$MnMoO_4$ hybrid electrodes was more excellent than $NiCo_2O_4$ electrodes, as shown in Fig. 10(g).

The conductivity of $NiCo_2O_4$ is two orders of magnitude larger than NiO or Co_3O_4, but it is necessary to explore the effects of the combination between $NiCo_2O_4$ and other oxides on the electrochemical performance. In fact, the $NiCo_2O_4$ composites are also potential candidates for high-performance supercapacitor. $NiCo_2O_4$, NiO, ZnO and Co_3O_4 were P-type semiconductors with the energy band gap of 2.1 [139], 3.6 [140], 3.37 [141] and 2.2 eV [142], respectively. To forecast the electrochemical performance of these transition metal oxides electrode materials, it is necessary to consider essential influences, such as pore structure [143–146], the electrical conductivity [147,148] and the degree of crystallization [149,150]. The electrical conductivity of transition metal oxides can be improved by changing band effects, and the improved electronic conductivity can usually the improve charge-transfer processes and reduce internal resistance of the electrodes [151,152]. The electrochemical activity of metal oxides usually depends on the crystallinity. The appropriate microstructure will contribute high specific surface area and the electrolyte permeation [153–155]. Interestingly, smarter integrated architectures combined with different genres of materials, such as MnO_2, NiO, and Co_3O_4, possess many competitive advantages, including rich approachable electroactive sites, high electron aggregation efficiency, short ion transfer pathways, and even excellent synergetic effects or multifunctional properties of the nanostructure components [156]. For these reasons, it is vital to coordinate microstructure, crystallinity, and electrical conductivity of these metal oxides-based materials for their potential application in ECs. In summary, researchers manifest that the fabrication of oxides composite with unique structure is an effective way to improve electrochemical behavior of the electrodes.

Recently, Zhou et al. [157] successfully anchored two types hierarchical core–shell arrays, namely, homogeneous $NiCo_2O_4$ nanosheet@$NiCo_2O_4$ nanorod and heterogeneous $NiCo_2O_4$ nanosheet@NiO nanoflake ($NiCo_2O_4$ sheets regard as the core skeleton for bearing shell materials) via facile solution hydrothermal methods and chemical bath deposition process in combination with a simple thermal treatment. $NiCo_2O_4$ nanorods disperse on the $NiCo_2O_4$ nanosheets in many directions. $NiCo_2O_4$ nanorods

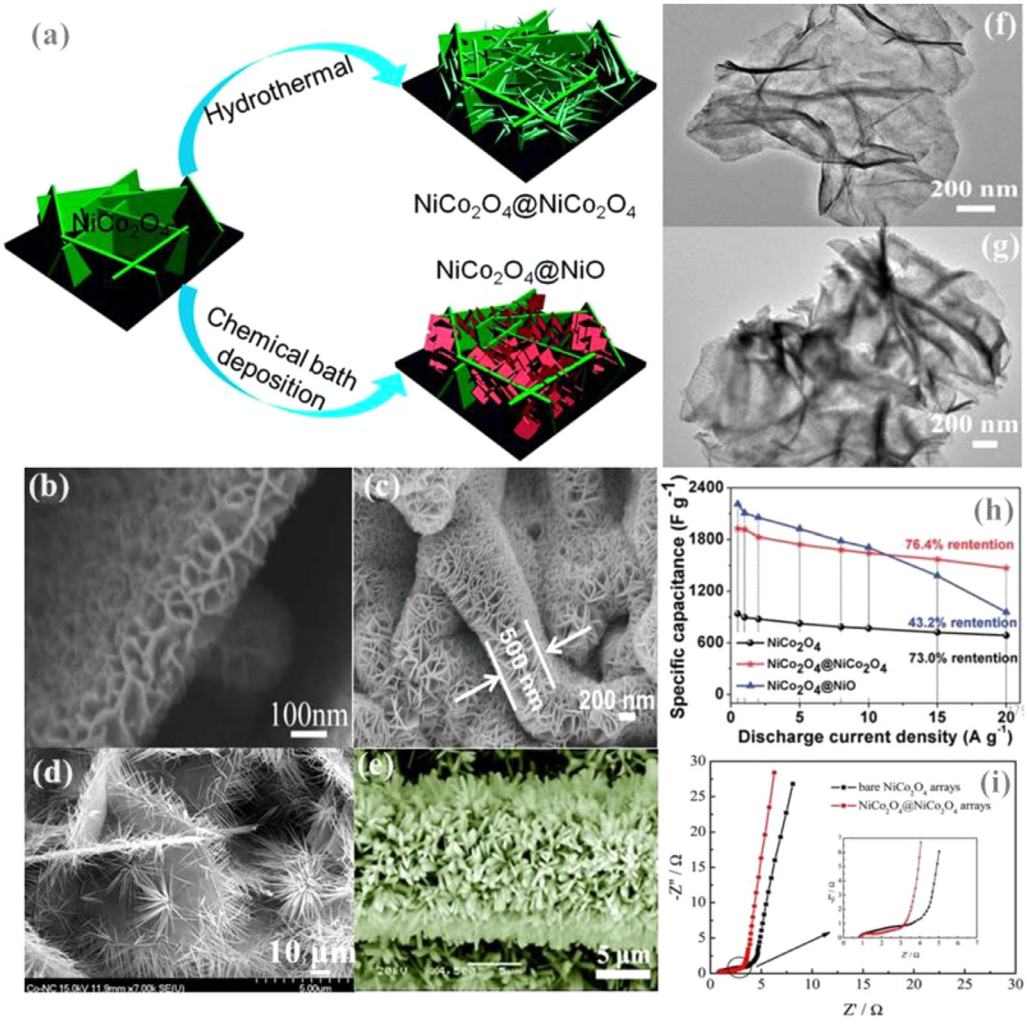


Fig. 11. (a) Schematic illustration of the controlled synthesis of homogeneous $NiCo_2O_4$ nanosheet@$NiCo_2O_4$ nanorod and heterogeneous $NiCo_2O_4$ nanosheet@NiO nanoflake core–shell nanoarrays [157], (b) SEM image of hierarchical $NiCo_2O_4$@$NiCo_2O_4$ core–shell heterostructured nanowire arrays on Ni foam substrate [158], (c) SEM images of $NiCo_2O_4$@MnO_2 core–shell nanosheet arrays [161], (d) SEM images of the 1D $NiCo_2O_4$ nanorods grown over and below the Co_3O_4 nanosheets [160], (e) SEM images of hierarchical $NiCo_2O_4$@NiO core–shell heterostructured nanowire arrays on CC substrate [159], (f) HRTEM images of as-synthesized $NiCo_2O_4$ nanosheet [161], (g) HRTEM images of as-synthesized $NiCo_2O_4$@MnO_2 nanosheet [161], (h) SC of the electrodes as a function of current density [157] and (i) Nyquist plots of bare $NiCo_2O_4$ and $NiCo_2O_4$@$NiCo_2O_4$ electrode [158]. Reproduced from Refs. [157,159] with permission from The Royal Society of Chemistry. Reproduced from Ref. [158] with permission from American Chemical Society. Reproduced from Refs. [160,161] with permission from Elsevier.

and $NiCo_2O_4$ nanosheets are interconnected. Similarly, for the $NiCo_2O_4$@NiO hybrid nanoarrays, the whole nanosheets obviously become thicker and the surfaces are fully covered by plentiful leaf-like NiO nanoflakes, forming a highly porous core–shell structure with convenient ion/electron transport paths, enhanced reactivity, and improved structural stability (Fig. 11a). When the two as-synthetized hierarchical nanoarrays were evaluated as supercapacitor electrodes, they exhibited high specific capacitance and enhanced rate capability, and improved cycling stability. It is observed from Fig. 11(h), that the specific capacitances retentions of $NiCo_2O_4$@$NiCo_2O_4$ and pristine $NiCo_2O_4$ nanosheets are 76.4% and 73% when the current densities fall from 0.5 to 20 A g^{-1}, and both electrodes are higher than the $NiCo_2O_4$@NiO (43.2%). If excessive amounts of NiO nanoflakes cover the $NiCo_2O_4$ nanosheets, the formed NiO shell will impede electrolyte diffusion during rapid charge/discharge processes, resulting in the low electrochemical performance of $NiCo_2O_4$@NiO. Even so, the $NiCo_2O_4$@NiO nanoarrays also exhibit higher specific capacitances (955 F g^{-1}) than the bare $NiCo_2O_4$ nanosheets (685 F g^{-1}) at high current density of 20 A g^{-1}. Hierarchical $NiCo_2O_4$@$NiCo_2O_4$ core/shell nanoflake arrays (Fig. 11b) were also synthesized by Liu et al. [158] via the facile hydrothermal and chemical bath deposition for high-performance supercapacitor materials. The TEM images of $NiCo_2O_4$ nanosheets arrays and $NiCo_2O_4$@MnO_2 core–shell nanosheet arrays were displayed in Fig. 11(f and g). Notably, $NiCo_2O_4$ nanosheets with wrinkles are beneficial to the composite between $NiCo_2O_4$ nanosheets and MnO_2 nanosheets because of the enhanced specific surface area. In addition, it seems that the $NiCo_2O_4$ nanosheets were covered with ca. 40–70 nm MnO_2 nanosheets. As shown in Fig. 11(i), the effective electron transfer and faster ion diffusion in the core/shell nanoflake arrays are further verified by the EIS measurements. The semicircle of the Nyquist plot corresponds to the Faradic reactions and its diameter stands for the interfacial charge-transfer impendence, and the result indicates that the interfacial charge-transfer impendence of the $NiCo_2O_4$@$NiCo_2O_4$ core/shell nanoflake arrays is smaller than that of the bare one. It is noteworthy that the framework of the 3D $NiCo_2O_4$@NiO structure with huge amounts of mesopores offers a shortened diffusion distance for electrons/ions, which improves the full use of the high pseudocapacitance of $NiCo_2O_4$@NiO and relieves the tension caused by the volume change and phase transformation [159]. Sennu group [160] also reported the preparation of high

energy asymmetric supercapacitor (ASC) adopting pseudocapacitive 3D microstructured composite $NiCo_2O_4$@Co_3O_4 and double layer forming activated carbon (AC), obtained from the bio-waste. The $NiCo_2O_4$@Co_3O_4 consisted of rod-like $NiCo_2O_4$ microstructure was grown on full surfaces of Co_3O_4 nanosheets (Fig. 11d). The ASC could deliver a high energy density of 42.5 Wh kg^{-1} and power density of 80 W kg^{-1}. Additionally, the ASC provides excellent cycle ability, the capacitance retention maintains ~97% of initial capacitance after 7000 cycles. A novel hierarchical $NiCo_2O_4$@MnO_2 core–shell nanosheet arrays composite directly grown on nickel foam formed integrated electrode for supercapacitors was designed and fabricated through simple two-step hydrothermal method [161]. Remarkably, it is discovered that the density of MnO_2 nanosheets has been increased as the extended reaction time. When the reaction time of MnO_2 nanosheets deposited on bare $NiCo_2O_4$ nanosheet lasts for 9 h, the particle size of a core–shell nanostructure is about 500 nm (Fig. 11c). The unique nanostructure has high electrochemical performance, displaying a capacitance of 2.39 F cm^{-2} as well as excellent cycling stability, which is superior to the pure $NiCo_2O_4$ nanosheet arrays. In these above electrode design, not only both the "core" and "shell" active materials can be fully utilized but also a strong synergistic effect can come true.

3.2.2. $NiCo_2O_4$-conducting polymer composites

In 1976, conducting polymers with good electric conductivity, large capacitance, low cost was discovered and then applied in capacitors. The conducting polymers is an important genre of electrode material for pseudocapacitors [162]. In the past few years, great effort has been devoted to conducting polymers owing to their huge latent applications in supercapacitors. Commonly, the most commonly used conducting polymers often include polypyrrole (PPy), polyaniline (PANI), and poly [3, 4-ethylenedioxythiophene] (PEDOT) and their derivatives [163]. Conducting polymers can be compounded via chemical and electrochemical methods, which are operated by polymerization of the monomer. In general, these polymers have several redox states from insulator to metal, which could be used in supercapacitors with a pseudocapacitance mechanism [164]. Commonly, conducting polymer possess a very relative large specific capacitance compared with the clear majority carbon materials, e.g., 1284 F/g for PANI, 480 F g^{-1} for PPy, and 210 F g^{-1} for PEDOT [165]. Moreover, works would pay more attention to their advantages, such as relatively low cost, environment-friendly, high charge density, and high electrical conductivity in doped states.

Recently, great efforts have been taken to increasing the capacitance of $NiCo_2O_4$ through exploring miscellaneous nanostructures to provide huge specific surface area and shorten ion diffusion path [166,167]. However, the poor conductivity problem of $NiCo_2O_4$ is still limited its further applications. The conducting polymer, like polyaniline (PANI), due to the high theoretical capacitance (up to 3407 F g^{-1}), controllable electrical conductivity, low cost and facile synthesis has drawn intensive attention among various pseudocapacitive materials [168]. Ppy is also a desired electrode material with high charge density and superior electrical conductivity in doped states (10 – 100 S cm^{-1}), which has also been widely adopted as electrode for SCs. For example, Ppy and PEDOT were wrapped up mesoporous $NiCo_2O_4$ nanosheet arrays via a facial and controllable electrodeposition process by Xu et al. [169]. Results indicate that the $NiCo_2O_4$@PPy electrode has the highest areal capacitance of 4.1 F cm^{-2} at 2 mA cm^{-2}, which is much higher than the values obtained for the $NiCo_2O_4$@PEDOT electrode (0.86 F cm^{-2}) and $NiCo_2O_4$ electrode (0.65 F cm^{-2}). What's more, even at high current density of 30 mA cm^{-2}, the areal capacitance of 2.7 F cm^{-2} can be achieved for $NiCo_2O_4$@PPy electrode. Moreover, the $NiCo_2O_4$@PPy electrode shows much smaller equivalent series resistance (ESR) than $NiCo_2O_4$@PEDOT and $NiCo_2O_4$ electrodes. By wrapping the highly conductive and porous polymer support, the distinct core-shell heterostructure is available for the best use of the pseudocapacitive behavior of PANI layer, offering a feasible measure to develop high-performance electrodes for supercapacitors [170]. Additionally, conducting polymers have reversible electrochemical redox properties, good environmental stability and strong charge storage capacity, especially, high electrical conductivity. Recently, conducting polymer-metal nanocomposites are widely researched as electrode materials because of their excellent stability under universal environmental conditions, good electrical conductivity and compatibility with high charge density, which has also been widely adopted as electrode material for high performance SCs by solving the poor electron transport and ion diffusion issues [171].

Typically, in the synthesis process, self-supported $NiCo_2O_4$ NWAs on carbon textiles were prepared by a modified hydrothermal growth method, and then the PPy or other conducting polymers was fabricated by the polymerization of pyrrole monomer and related reagent via carried out at 0 – 5 °C. For example, the synthesis of 3D hierarchical $NiCo_2O_4$@PPy coaxial nanowire arrays on carbon textiles as electrode for high-performance SCs was first reported by Kong group [172]. As shown in Fig. 12(a), the inlayer mesoporous $NiCo_2O_4$ nanowires work as the "core" with high capacitance and the coated PPy nanospheres serve as the "shell" with excellent conductivity. The 3D PPy nanospheres coupled with 3D $NiCo_2O_4$ nanowire arrays ($NiCo_2O_4$@PPy NWAs) electrode exhibit a high specific capacitance (~2244 F g^{-1}) at the current density of 1 A g^{-1} in 3 M KOH aqueous solution, excellent rate capability of ~60.5% and good cycling stability with the capacity retention of 89.5% after 5000 cycling as well as 82.9% after 10,000 cycling (Fig. 12d and e). The $NiCo_2O_4$@PPy NWAs obtained after 1.5 h polymerization exhibit the highest specific capacitance and lowest internal resistance (IR) among all samples. The (IR) of the $NiCo_2O_4$@PPy NWAs hybrid electrode was ~0.016 V, which is much smaller than that of the $NiCo_2O_4$ NWAs electrode (0.03 V). The result shows that the PPy shell can effectively reduce the total resistance and thus improve the charge transport and electron collection efficiency. However, the thick and dense PPy layer could prevent the ion penetration to the inner core of $NiCo_2O_4$ NWAs. As a result, the PPy polymerization time is a key factor in the design of high-performance $NiCo_2O_4$@PPy electrode.

Compared with PPy, PANI has a much higher theoretical capacitance. Furthermore, ordered PANI nanowire arrays are supposed to have a good capacitance performance owing to their special structure [173]. A reasonable design with an easy synthesis of PANI-based composite electrode has been realized by constructing novel core-shell architecture and adopting porous $NiCo_2O_4$ nanorod arrays as substrate. Typical structures of the $NiCo_2O_4$@PANI NRAs (Fig. 12b and c) were synthesized by Jabeen's group [174]. It can be found that the surface of $NiCo_2O_4$ NRAs is thoroughly covered with a thin PANI film (about 40 nm), indicating a representative core – shell heterostructure. As displayed in Fig. 12(f), the mean capacitance retention achieved as high as 91 ± 4% at 10 A g^{-1} after 3000 continuous cycles in 1 M H_2SO_4 aqueous solution. The super cycling stability can be ascribed to the optimized synergetic effects and logical design of the patent core – shell $NiCo_2O_4$@PANI NRAs. The inset in Fig. 12(f) suggests typical charge – discharge plots from the 3000 successive cycles. The curves were symmetric corresponding to charge – discharge process, demonstrating no significant structural collapse of the $NiCo_2O_4$@PANI NRAs electrode. Generally, the metal/conductive polymer composite electrode materials with unique core-shell structure are easy to be prepared. In the meantime, the high capacitance of metal oxides can be fully achieved. The microscale supercapacitors can meet the energy demand of different electronic devices on chips. The combination

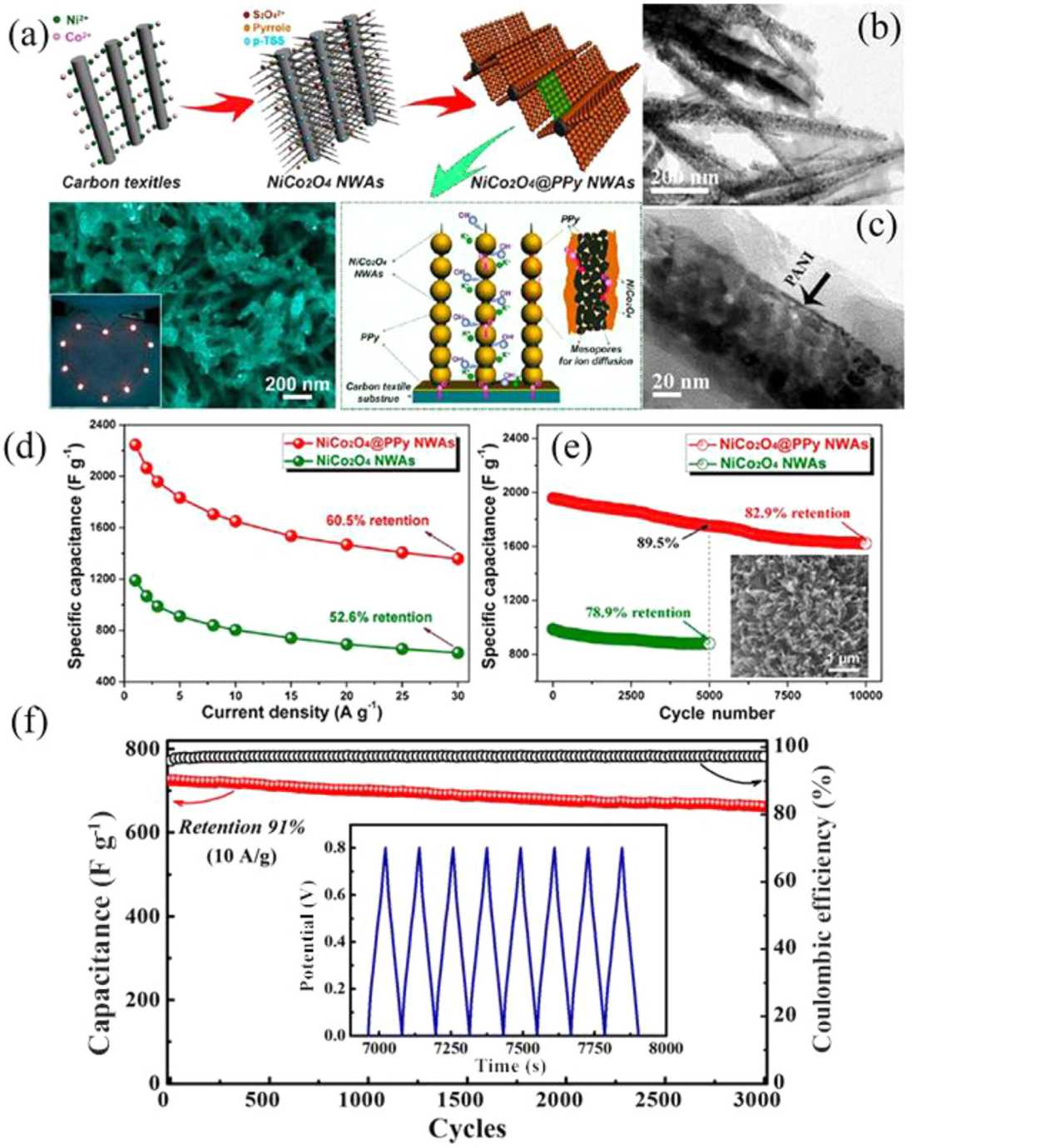


Fig. 12. (a) Schematic illustration of the fabrication process of hierarchical mesoporous $NiCo_2O_4$@PPy hybrid NWAs on carbon textiles (left: $NiCo_2O_4$@PPy NWAs top view; right: schematic representation of rechargeable supercapacitor based on $NiCo_2O_4$@PPy NWAs on carbon textiles) [172], (b) TEM images of the $NiCo_2O_4$@PANI NRAs, (c) an individual core – shell nanorod [174], (d) current – density dependence of the specific of the $NiCo_2O_4$ NWAs and $NiCo_2O_4$@PPy NWAs electrode [172] and (e) cycling performance of the $NiCo_2O_4$@PPy NWAs electrodes (10,000 cycles), compared to $NiCo_2O_4$ NWAs electrodes (5000 cycles) [172]. (f) Cycle performance of the $NiCo_2O_4$@PANI NRAs electrode for 3000 successive charge – discharge cycles at a large current density of 10 A g^{-1} and corresponding Coulombic efficiency (inset is the typical charge – discharge curves) [174]. Reproduced from Refs. [172,174] with permission from American Chemical Society.

of new functions between metal oxides and conductive polymer composites could further widen the application field of supercapacitors.

3.2.3. $NiCo_2O_4$-MOFs (metal-organic frameworks) composites

The discovery of metal–organic frameworks (MOFs), as a new class of crystalline porous materials (CPMs) with high surface areas, remarkable porosity, enormous structure diversity, and multifunctional tunability with accuracy at the molecular level has unlocked the potential opportunities for scientists to solve some pressing problems related to sustainable energy, adsorption, sensors, supercapacitors, and catalysts [175]. MOFs are assembled by joining inorganic metal nodes (secondary building units, SBUs) with organic linkers (Fig. 13a), which are consisted of metal ions and organic binding ligands and have increasingly drawn urgent attention [176–178]. The pseudocapacitance behavior can be found in MOFs, and pseudocapacitive MOFs are mainly from 3d transition metals, where the metal nodes supply the redox activity

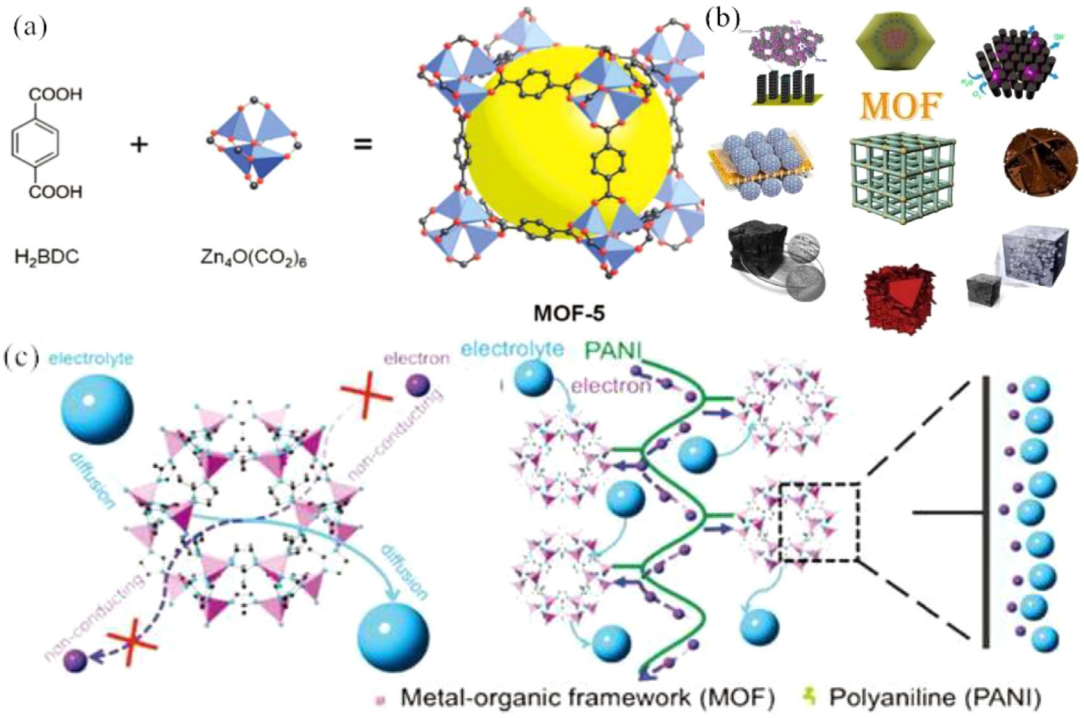


Fig. 13. (a) Building blocks and crystal structures of MOF-5 [179], (b) examples of some MOF-based nanostructures [191] and (c) schematic representation of electron and electrolyte conduction in MOF and MOF interwoven by PANI [175]. Reproduced from Refs. [175,191] with permission from The Royal Society of Chemistry. Reproduced from Ref. [179] with permission from American Association for the Advancement of Science.

[179]. Compared with familiar inorganic porous materials, their crystalline structures with high-porosity, larger specific surface areas, diversity of structures and controllable functionalities [180–186]. Recently, owing to their porous structures with high surface areas, MOFs have been used as desired sacrificial templates to support various porous active materials, such as carbonaceous materials, metal oxides, and metal phosphides [187–191]. In addition, its structure is novel and strange. As shown in Fig. 13(b), the as-prepared products of metal oxides/hydroxides with various structures, such as hollow nanocages, nanoframes, multishelled microboxes, can be obtained [192–196].

MOFs are promising porous precursors for the construction of various functional materials for high-performance electrochemical energy storage and conversion system because they can offer abundant active sites and shorten ion diffusion distance as well as relax the tension during the electrochemical reactions, thus keeping the wholeness of the electrodes [197–205]. For making use of the advantage of MOF materials possibly and well, it is necessary to further study situation of all sides in supercapacitors. In recent years, Wang et al. covered the recent research advancement in utilizing MOFs and their composites or derivatives by focusing on the relationship of architecture, composition, and function for energy storage and conversion systems [206]. Choi et al. [207] reported the electrochemical performance of M7M-MOF-74 containing seven different metal elements, such as Co, Mg, Ni, Zn, Mn, Fe and Cd. For example, a novel hollowed cubic NiS nanoframe electrode was synthesized by anion exchange of a Ni-Co MOF with S^{2-} ions, which exhibited improved electrochemical performance in supercapacitors [208]. According to early research, it is noteworthy to explore the effect of surface properties of MOFs on their capacity of charge storage. For this purpose, Lee et al. [209] studied Co MOFs with different pore dimensions and morphology and reported the influence of pore dimensions and morphology on the supercapacitive performance, which is under the guidance of coordination copolymerization of topologically different linkers with identical coordinating functionality. Wang et al. [210] reported a novel tactic for fabricating high performance SCs and solved the insulating problems of MOFs by introducing polyaniline (PANI) chains into Co-MOF crystals (ZIF-67) (Fig. 13c) with an extraordinary areal capacitance of 2146 mF cm^{-2} at 10 mV s^{-1}. Recently, Hu et al. developed a MOFs template-engaged method to prepare multicompositional Fe_2O_3-SnO_2 microboxes, and it exhibited more excellent lithium storage performance than the single-compositional micro-boxes [211]. Notably, a kind of amphoteric metal oxide (such as ZnO) can be dissolved in acid or alkali, which impedes its extensive applications as an excellent electrode material in SCs [212–214]. To solve this problem, Zeng and co-workers [215] introduce a metal-organic framework (MOF) structure to effectively protect the ZnO nanorods from corrosion in the alkali electrolyte such as KOH or NaOH solution. Ultimately, the carbon coating ZnO nanorods array derived from zeolitic imidazole framework-8 (ZIF-8) was obtained (Fig. 14d and e). Cao et al. [216] reported a facile two-step solution method to design a novel hollow $NiCo_2O_4$ nanowall arrays electrode on flexible carbon cloth substrate (Fig. 14a and b). As exhibited in Fig. 14(c), it is obvious that the hollow characteristic is presented clearly by the top cross section, and the surface of the nanowall arrays has been wrapped with cross-linked ultrathin nanoflakes. These results show that hollow and porous structure is successfully prepared on the carbon cloth. The as-obtained $NiCo_2O_4$ nanostructure arrays can provide rich reaction sites and shorten ion diffusion path. When evaluated as a flexible electrode material for supercapacitor, the as-fabricated $NiCo_2O_4$ nanowall electrode shows remarkable electrochemical performance with excellent rate capability and long cycle life. In addition, the hollow $NiCo_2O_4$ nanowall electrode exhibits promising electrocatalytic activity for oxygen evolution reaction. The CC@ $NiCo_2O_4$ exhibits a high capacitance of 1055.3 F g^{-1} at a small current of 2.5 mA cm^{-2} and a high capacitance of 483.3 F g^{-1} at the current density increased to 60 mA cm^{-2}. The capacitance retention can reach 45.8% even the

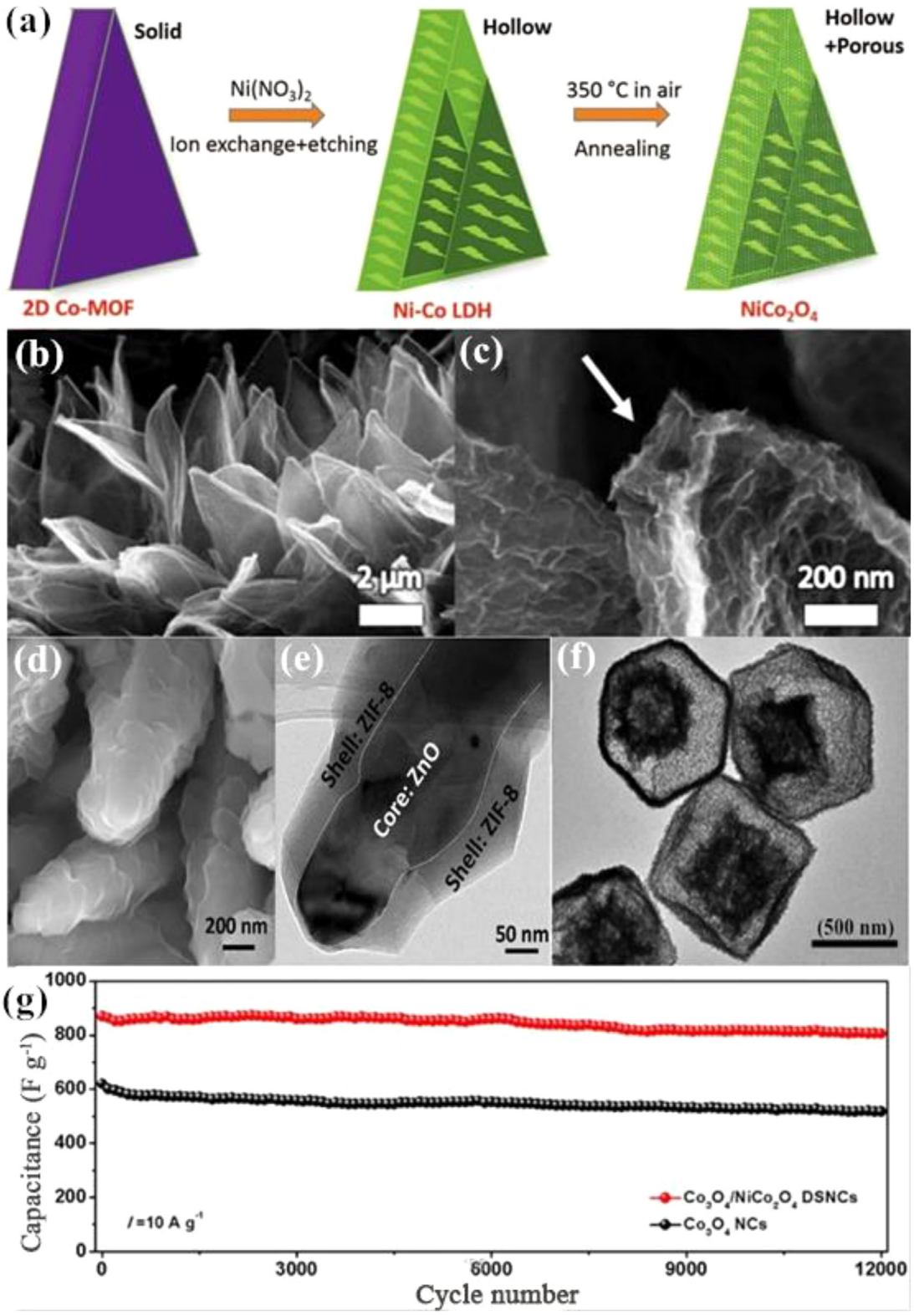


Fig. 14. (a) Schematic illustration of the formation of hollow $NiCo_2O_4$ nanostructure from 2D Co-MOF solid nanowalls [216], (b, c) $NiCo_2O_4$ hollow nanostructure. The arrows in (c) indicate the hollow feature of the materials [216], (d) high magnifications SEM of ZnO@ZIF-8 core-shell NRs grown on flexible cloth [215], (e) high resolution TEM images of a ZnO@ZIF-8 core-shell nanorod [215], (f) TEM image of an individual $Co_3O_4/NiCo_2O_4$ DSNC [217] and (g) cycling performance at a current density of 10 A g^{-1} [217]. Reproduced from Refs. [215,217] with permission from The Royal Society of Chemistry. Reproduced from Ref. [216] with permission from Wiley-VCH.

current increased 24 times. Additionally, hollow structures with high complexity in shell architecture and composition have attracted tremendous interest because of their great importance for both fundamental studies and practical applications. Recently, Hu et al. [217] reported the synthesis of novel box-in-box nanocages (NCs) with different shell compositions, namely, $Co_3O_4/NiCo_2O_4$ double-shelled nanocages (DSNCs). The particles still retain a polyhedral shape but exhibit a rougher surface constructed by small nanosheets, as shown in Fig. 14(f). The $Co_3O_4/NiCo_2O_4$ DSNCs exhibits a high capacitance of 972 F g^{-1} at a current density of 5 A g^{-1} and an impressive capacitance of 615 F g^{-1} even at a current density of 50 A g^{-1}. This means that the capacitance retention can retain 63.2% even the current density increases from 5 to 50 A g^{-1}, indicating superior rate capability. Compared with $Co_3O_4/NiCo_2O_4$ DSNCs, the Co_3O_4 NCs delivers inferior performance in terms of much lower specific capacitance and poor rate capability. Furthermore, the electrochemical stability over cycling is evaluated at a current density of 10 A g^{-1} by repeated charging and discharging for 12,000 cycles. As shown in Fig. 14(g), the specific capacitance of 870 F g^{-1} for the first cycle gradually decreases to a value of 805 F g^{-1} after 12,000 cycles with a capacitance retention of 92.5%. The superior cycling stability is likely related to the excellent structural stability of the Co_3O_4/ $NiCo_2O_4$ DSN.

In general, the applications of transition-metal (Fe, Co, Ni) MOFs and their derivatives in supercapacitors and batteries are attracted by many researchers. The conductivity of most transition-metal (Fe, Co, Ni) based MOFs electrodes is poor. However, it could be enhanced by combining with materials of high conductivity such as conducting polymer, carbon nanotube, reduced graphene oxide. Additionally, MOFs material is a new type of multi-functional compound material which has many excellent properties the other materials do not have [218]. Hence, the composite between MOFs and $NiCo_2O_4$ electrode usually shows unique characteristic.

3.2.4. $NiCo_2O_4$-metal sulfide composites

Transition metal oxides and their compounds are widely applied to supercapacitors due to their high abundance, high theoretical capacitances (> 1000 F g^{-1}) and environmentally friendly. However, the low intrinsic conductivity [219], inferior rate capability and poor cycling stability hindered the further practical applications in the field of energy storage [220]. In addition, the rate capability and efficiency of $NiCo_2O_4$ electrode material are still unacceptable despite its remarkable high theoretical capacitance. The rate capability of the electroactive material, as well-known, is principally determined by the kinetics of ion diffusion and electron transport, electronic conductivity [221]. Whereas, transition metal sulfides (TMS), especially nickel sulfide (Ni_2S_3, etc.), cobalt sulfide (Co_9S_8, Co_3S_4, etc.) and AB_2S_4 (A and B = Fe, Co, Ni, etc.) spinel structures bimetallic sulfides were generally served as the promising pseudocapacitive electrode materials owing to their superior electrical conductivity and high electrochemical activity [222,223]. Moreover, the synthesis methods of sulphide are usually simple. Such metallic sulfides with unique and variable morphologies can be easily transformed from their corresponding metal oxide/hydroxide precursors by anion exchange reactions and Kirkendall effects. Therefore, a combination between transition metal oxides and sulphides has drawn much attention as excellent pseudo-capacitors materials owing to their excellent electrical conductivity and more available metal oxidation states to further redox reactions. As a result, various metal sulfides have been introduced into the $NiCo_2O_4$ material to form composite materials, and the rate capability performance and cycling stability of $NiCo_2O_4$ can be obviously improved due to the synergistic effect. For example, as shown in Fig. 15(a), Chu et al. [224] have reported that electrodeposition of nickel sulfide (Ni-S) on $NiCo_2O_4$ ($NiCo_2O_4$@Ni-S) nanoplate arrays forms a novel hierarchical $NiCo_2O_4$@NiS functional-material, which delivers high specific capacitances of 1.85 F cm^{-2} at 8 mA cm^{-2}. As can be seen, the $NiCo_2O_4$ nanoplate has a width of about 30 nm, and a thickness ranging from 0.5 to 1.5 nm. Ni-S nanoplates were uniformly covered by a thin layer nanostructure, forming thicker core-shell $NiCo_2O_4$@Ni-S nanoplate arrays. Three-dimensional hierarchical core/shell nanostructure is favourable for faster ion and electron transfer owing to large specific areas and small bandgaps for anion exchange. Consequently, $NiCo_2O_4$@Ni_3S_2 core/shell arrays [225,226], can be synthesized by stepwise synthesis approach, which includes hydrothermal synthesis and electrodeposition or hydrothermal sulfurization process. Moreover, Fig. 15(d and g) confirms that the $NiCo_2O_4$@Ni_3S_2 has a core/shell nanostructure, and it makes the $NiCo_2O_4$ as the core and Ni_3S_2 as the shell. In addition, 3D hierarchical $NiCo_2O_4$ nanosheets/Co_3S_4 nanoneedle hybrid nanostructure were synthesized firstly by Shi's group [227]. The optimized $NiCo_2O_4/Co_3S_4$ electrode shows excellent pseudocapacitor behaviors with high specific capacity of 1468 F g^{-1} (1 A g^{-1}). Co_3S_4 nanoneedles can be observed attached tightly on the surface of $NiCo_2O_4$ (Fig. 15e), which can increase the specific surface area and shorten the diffusion path of ions and electrons during electrochemical reaction process. TEM image in Fig. 15(f) further confirms that the detailed microstructure of composite electrode material is composed of Co_3S_4 nanoneedles and $NiCo_2O_4$ nanosheets. It's noteworthy that MoS_2 exhibits greatly enhanced electrical conductivity due to the intrinsic small bandgaps for the anion exchange [228]. MoS_2 nanowires/$NiCo_2O_4$ nanosheets hybrid nanostructure grown on Ni foam network as binder-free composite electrode was prepared through a facile hydrothermal method [229]. As displayed in Fig. 15(b and c), the $NiCo_2O_4$ nanosheets stick to the Ni foam surface, which can offer a mass of sites to grow MoS_2 nanowires. The nanowires and nanosheets are twined together to form composites, and then restrain the agglomeration of nanosheets. Hence, the specific surface area is increased, and the transport path of ions/electrons is shortened. Notably, compared with corresponding single-component nickel sulphides and cobalt sulphides, $NiCo_2S_4$ possesses more redox reactions with mixed valence state [230]. It also shows lower optical band gap energy than $NiCo_2O_4$ [231]. Importantly, it shows high electrical conductivity of $\sim 1 \times 10^3$ S cm^{-1} [232], which is about 100 times as much as $NiCo_2O_4$. Interestingly, three-dimensional $NiCo_2O_4/NiCo_2S_4$ hybrid nanostructure on Ni-foam as a conductive substrate by a facile ammonia evaporation technique, exhibited a striking specific capacitance of 3671 F g^{-1} at a current density of 1.8 A g^{-1} and 2767 F g^{-1} at 9 A g^{-1} with a capacity retention of 84% at 10 A g^{-1} after 2000 cycles [233]. These capacitance performances were much more superior to bare $NiCo_2O_4$ nanosheets (see Fig. 15h and i). It indicates that the synergistic effect between $NiCo_2O_4$ and $NiCo_2S_4$ improves the capacitance at the high current density due to the high electrical conductivity of $NiCo_2S_4$.

In general, both the $NiCo_2O_4$ with high theoretical capacity and metal sulfide with relatively good conductivity are good pseudocapacitive materials. The unique hierarchical core/shell nanostructures with enhanced mechanical stability would provide a short and fast transport pathway, thus accelerate the efficient electrochemical reaction process. It provides a feasible way to improve the electrochemical performance of other pseudo-capacitive materials in the future research development.

3.2.5. $NiCo_2O_4$-carbon based composites

Carbon materials such as templated porous carbons, carbon aerogels, carbon nanotubes, graphene [234–236], are the most commonly used supercapacitor materials. They possess large activated surface areas, excellent electrical conductivity, strong mechanical strength and high chemical stability however. However,

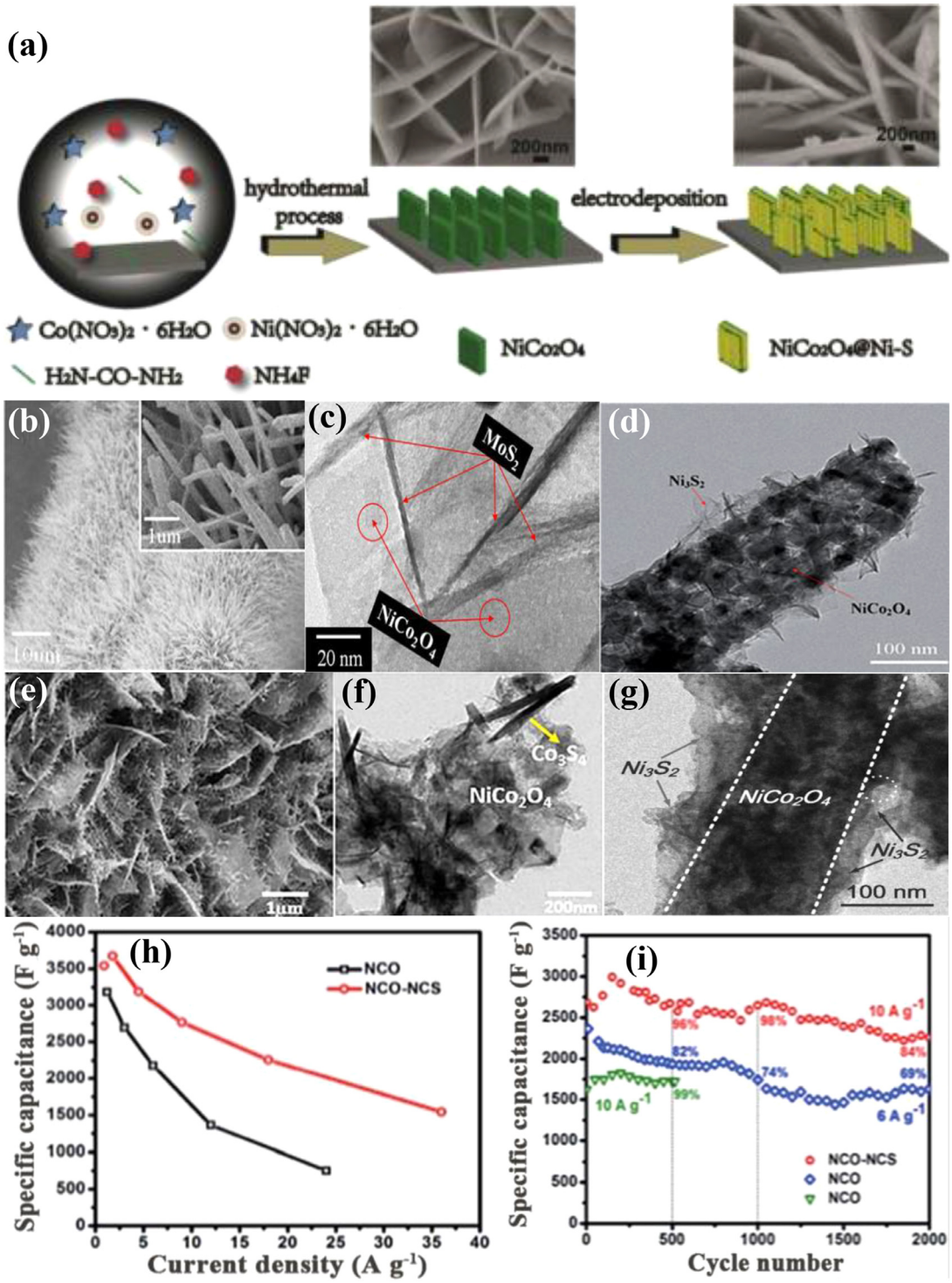


Fig. 15. (a) Schematic illustration of the two-step synthesis of hierarchical $NiCo_2O_4$@NiS core shell nanoplate arrays [224], (b) typical SEM images of the sample $MoS_2/NiCo_2O_4$ supported on Ni foam at different magnifications [229], (c) typical TEM image of the $MoS_2/NiCo_2O_4$ supported on Ni foam [229], (d) TEM of $NiCo_2O_4$ and $NiCo_2O_4$@Ni_3S_2 core/shell mesoporous nanothorn arrays [226], (e) typical SEM image of NC-6 [227], (f) typical TEM image of NC-9 [227], (g) the $NiCo_2O_4$@Ni_3S_2 hierarchical nanostructure [225], (h) summary of specific capacitance as a function of current densities [233] and (i) cycling stability of electrodes [233]. Reproduced from Refs. [224,227,229] with permission from Elsevier. Reproduced from Refs. [225,226,233] with permission from The Royal Society of Chemistry.

the specific capacitance of carbon is much lower than that of transition metal oxides, which limits their practical applications to a certain degree. Fortunately, carbon modification can improve the electrical conductivity of $NiCo_2O_4$-based electrode materials. In fact, various carbon additives such as carbon nanotubes (CNTs), graphene, have been introduced into the transition metal oxides material to form composite materials, and the rate capability performance and cycling stability of $NiCo_2O_4$ can be obviously improved due to the improved conductivity [237–239]. In conclusion, a combination between $NiCo_2O_4$ and carbon materials may take full advantage of the superior electrical conductivity and large specific surface areas of carbon materials as well as the high specific capacitance of $NiCo_2O_4$. So far, great efforts have been made in this field and the following section will describe briefly.

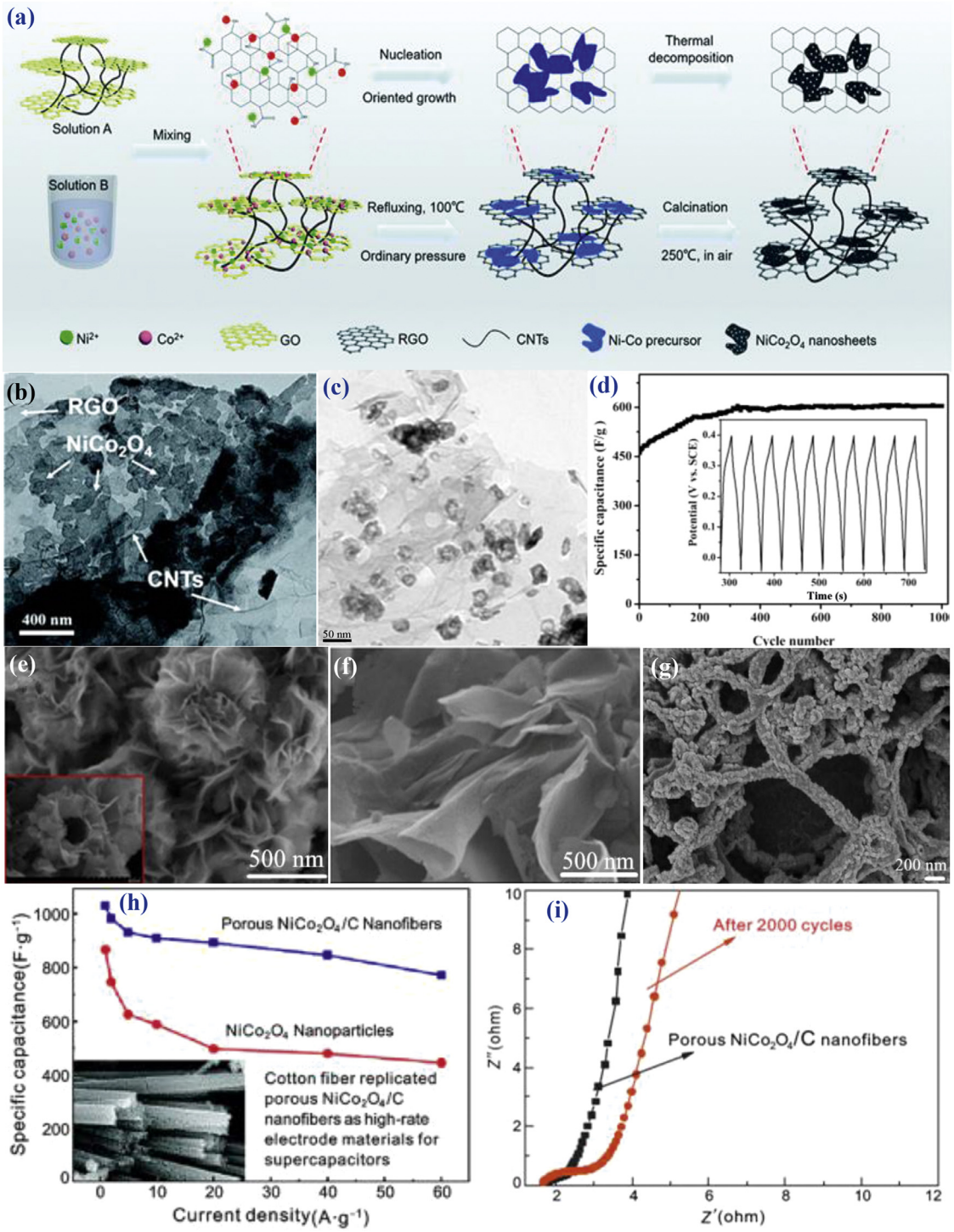


Fig. 16. (a) Scheme showing the synthesis of NCO NRs and RG/NCO NCs [242], (b) TEM image of the FCP-$NiCo_2O_4$/RGO/CNTs composite [242], (c) TEM image of hollow $NiCo_2O_4$/graphene composite [243], (d) cycle performance of the hollow $NiCo_2O_4$ nanoparicle/graphene composite [243], (e) SEM image of C@$NiCo_2O_4$ HSs [244], (f) SEM image of $NiCo_2O_4$ NSs [244], (g) FESEM images of as-prepared 3D $NiCo_2O_4$/CNT core–shell network structure [245], (h) comparison of specific capacitance between $NiCo_2O_4$ nanoparticles and porous $NiCo_2O_4$/C nanofibers at various scan rates (the inset is typical FE-SEM image for porous $NiCo_2O_4$/C nanofibers [246]) and (i) EIS curves of porous $NiCo_2O_4$/C nanofibers before and after 2000 cycles [246]. Reproduced from Refs. [243,244,246] with permission from Elsevier. Reproduced from Refs. [242,245] with permission from Royal Society of Chemistry.

Typically, graphene as a type of two-dimensional carbon with large specific area and high conductivity, has been investigated as electrode material incorporated with metal oxides [240,241]. Especially, $NiCo_2O_4$/graphene composite exhibited outstanding electrochemical performance owing to the synergetic effect between conductive graphene and high theoretical capacity of $NiCo_2O_4$. For example, Zhang *et al.* reported few-crystalline, porous $NiCo_2O_4$ nanosheets (FCP-$NiCo_2O_4$/RGO/CNTs) grown on graphene and carbon nanotubes synthesized in reflux at 100 °C for 12 h (Fig. 16a). The FCP-$NiCo_2O_4$/RGO/CNTs not only provide an effective charge transport path due to high conductive graphene and CNTs, but also avoid the aggregation of individual components and

facilitate the diffusion of charge/ions within the electrode. As can be seen in Fig. 16(b), there are lots of the $NiCo_2O_4$ nanosheets attached on the RGO surface to form porous structure, which is in favor of enhancing the charge storage capability of $NiCo_2O_4$ nanosheets [242]. The hollow $NiCo_2O_4$ nanoparticle/graphene composite was firstly prepared through a template-free method [243]. As shown in Fig. 16(c and d), the hollow $NiCo_2O_4$ nanoparticle/graphene composite presents high specific capacitance (1238 F g^{-1} at 1 A g^{-1}) and excellent cycle stability (604 F g^{-1} at 10A g^{-1} for 1000 consecutive cycles). In a subsequent study, Li et al. [244] prepared C@$NiCo_2O_4$ hollow microspheres (HSs) composite by a two-step strategy of hard-template method. Fig. 16(e and f) displays the SEM image of the C@$NiCo_2O_4$ material with and without templates, respectively. Obviously, an obvious morphology difference of both samples can be found, and the C@$NiCo_2O_4$ sample synthesized by template shows obvious core-shell structure. As shown in Fig. 16(g), $NiCo_2O_4$ nanoparticles were tightly grown on the sidewall of CNTs, forming a 3D core-shell network structure with open space size ranging from several hundred nanometers to several micrometers, resulting in much reduced specific surface area [245]. Carbon nanofibers (CNFs) are cylindric nanostructures with graphene layers, which also possess large specific surface area and high conductivity. Therefore, porous $NiCo_2O_4$/C nanofibers are synthesized with cotton as template via mild hydrothermal route [246]. As exhibited in Fig. 16(h), the porous $NiCo_2O_4$/C nanofibers deliver a specific capacitance of 1029 F g^{-1} at a current density of 1 A g^{-1}, which is much higher than that of bare $NiCo_2O_4$ nanoparticles. More notably, $NiCo_2O_4$/C nanofibers material shows remarkable rate capability. Even though the current density is up to 60 A g^{-1}, its specific capacitance still retains at 771 F g^{-1}. Obviously, the charge-transfer resistance (R_{ct}) of $NiCo_2O_4$/C nanofibers electrode is very low, indicating an efficient ion diffusion and rapid redox reaction process (see Fig. 16i).

At the end, taking full use of the good conductivity and high surface area of carbon materials are the key points in preparing $NiCo_2O_4$@C materials composite electrodes. The synergistic effects of $NiCo_2O_4$ and carbon nanomaterials can maximize the properties of different components, for example, to further improve the conductivity of the $NiCo_2O_4$ materials. The carbon coated $NiCo_2O_4$ nanocomposites have large surface areas, resulting in better electrolyte wettability and high conductivity, which contribute to cycling stability. Therefore, the excellent electrochemical performance and reasonable architectural design of $NiCo_2O_4$@C materials exhibits promising potential for practical application in energy storage.

4. Conclusions and perspectives

Generally, supercapacitors possess a very wide range in energy storage field applications prospect. Recent advances in frequently-used synthesis method and structures of $NiCo_2O_4$-based electrochemical capacitors, including pristine $NiCo_2O_4$ and their composites with diverse morphology, have been summarized in this review. The review emphasizes the advantages of $NiCo_2O_4$ as the materials of supercapacitors with super rate capability, high energy density, good power density, and excellent cycling stability. Meanwhile, we have advanced reasonable improvements in the electrochemical performance of $NiCo_2O_4$ electrode materials and anticipate that this review can facilitate further studies and advancements in this field:

(1) Many methods have been used to prepare $NiCo_2O_4$-based electrode materials, including sol-gel, bio-template, electrodeposition, electrospinning and hydrothermal methods. By comparison, the hydrothermal process is a direct and effective way to synthesize 1D, 2D and 3D nanostructured $NiCo_2O_4$-based materials with unique architectures and superior electrochemical performances by adjusting temperature parameters, the kinds and concentration of surfactants. Compared with 1D and 2D nanostructures, 3D structural morphology not only forms the desired hierarchical porous continuous channels for electrolyte ions by serving as an ion buffering reservoir, but also has higher electrical conductivity and excellent structural mechanical stability, which can alleviate the volume expansion effect during charge/discharge process.

(2) The electrochemical performance of $NiCo_2O_4$-based materials can be improved by controlling the pore properties and morphology. The novel nanostructures such as hollow, core-shell and hollow-core-shell are explored to further improve the electrochemical performances with feasible approaches. $NiCo_2O_4$-based materials with 3D hierarchical core-shell structure have attracted much attention because of the high surface/volume ratios, larg surface areas, excellent permeabilities and more surface-active sites, which is vital to achieve high energy/power densities in electrochemical supercapacitors.

(3) The electrochemical performance of $NiCo_2O_4$-based materials can be improved by taking full advantage of the synergistic effects of $NiCo_2O_4$ and other metal oxides, sulfides, conducting polymers or carbon nanomaterials. The synergistic effects can maximize the properties of different components, for example, to further improve the conductivity or capacity of the $NiCo_2O_4$ materials.

(4) The spinel $NiCo_2O_4$ shows high performance, but there still are many challenges to be conquered before commercialization. In concept, the $NiCo_2O_4$ material as a hybrid supercapacitor or battery-type supercapacitor is being in controversy. There is no doubt that high theoretical capacitance of spinel $NiCo_2O_4$ was known very well. In addition, the working voltage window of $NiCo_2O_4$ in alkali electrolyte is only approximately 0.45–0.5 V, which shows a relatively low energy and power density. Therefore, it is necessary to assemble with a carbon material into an asymmetric capacitor to build a stable and higher operating voltage window.

In general, $NiCo_2O_4$-based supercapacitor devices may play a critical role in renewable energy, and it may be expected to solve environmental pollution problems and reduce the use of hydrocarbon fuels. With rapid development of $NiCo_2O_4$-based electrodes, the high-performance supercapacitors with safe operation and friendly environment are suitable as practical energy storage devices. Therefore, the excellent electrochemical performance and reasonable architectural design of $NiCo_2O_4$-based materials exhibits promising potential for practical application in energy storage.

Acknowledgments

This work was financially supported by the National Natural Science Foundation of China (nos. 51774002 and 51672156), and Anhui Provincial Science Fund for Excellent Young Scholars (no. gxyqZD2016066), the National Key Basic Research Program of China (2014CB932400), Guangdong special support program (2015TQ01N401), Shenzhen Technical Plan Project (KQJSCX20160226191136).

References

[1] S. Chu, A. Majumdar, Nature 488 (2012) 294–303.
[2] J. Lv, T. Liang, M. Yang, S. Ken, M. Hideo, J. Energy Chem 26 (2017) 330–335.
[3] B.D. Boruah, A. Misra, J. Mater. Chem. A 4 (2016) 17552–17559.
[4] Y. Tu, D. Deng, X. Bao, J. Energy Chem 25 (2016) 957–966.
[5] T. Brezesinski, J. Wang, S.H. Tolbert, B. Dunn, Nat. Mater. 9 (2010) 146–151.
[6] C. Liu, F. Li, L.P. Ma, H.M. Cheng, Adv. Mater. 22 (2010) E28–E62.
[7] Q. Zhang, B. Zhao, J. Wang, C. Qu, H. Sun, K. Zhang, M. Liu, Nano Energy 28 (2016) 475–485.

[8] M. Armand, J.M. Tarascon, Nature 451 (2008) 652–657.
[9] M.S. Whittingham, Chem. Rev 104 (2004) 4271–4302.
[10] B.E. Conway, J. Electrochem, Soc. 138 (1991) 1539–1548.
[11] E. Frackowiak, Phys. Chem. Chem. Phys. 9 (2007) 1774–1785.
[12] H. Jiang, P.S. Lee, C. Li, Energy Environ. Sci. 6 (2013) 41–53.
[13] Q. Meng, K. Cai, Y. Chen, Y. Chen, L. Chen, Nano Energy 36 (2017) 268–285.
[14] C. Largeot, C. Portet, J. Chmiola, P.L. Taberna, Y. Gogotsi, P. Simon, J. Am. Chem. Soc. 130 (2008) 2730–2731.
[15] J. Yan, Q. Wang, T. Wei, Z. Fan, Adv. Energy Mater. 4 (2014) 157–164.
[16] Z. Yu, L. Tetard, L. Zhai, J.Y. Thomas, Energy Environ. Sci. 8 (2015) 702–730.
[17] G. Yu, X. Xie, L. Pan, Z. Bao, Y. Cui, Nano Energy 2 (2013) 213–234.
[18] L. Hu, W. Chen, X. Xie, N. Liu, Y. Yang, H. Wu, Y. Yao, M. Pasta, Y. Cui, H.N. Alshareef, ACS Nano 5 (2011) 8904–8913.
[19] L. Nyholm, G. Nyström, A. Mihranyan, M. Strømme, Adv. Mater. 23 (2011) 3751–3769.
[20] A. Huang, J. Yan, H. Zhang, X. Li, H. Zhang, J. Energy Chem. 26 (2017) 121–128.
[21] L. Wei, H.E. Karahan, S. Zhai, Y. Yuan, Q. Qian, K. Goh, A.K. Ng, Y. Chen, J. Energy Chem. 25 (2016) 191–198.
[22] X. Wang, M. Wang, X. Zhang, H. Li, X. Guo, J. Energy Chem. 25 (2016) 26–34.
[23] Y. Zhai, Y. Dou, D. Zhao, P.F. Fulvio, R.T. Mayes, S. Dai, Adv. Mater. 23 (2011) 4828–4850.
[24] X. Zhang, H. Zhang, Z. Lin, M. Yu, X. Lu, Y. Tong, Sci. China Mater. 59 (2016) 475–494.
[25] V. Augustyn, P. Simon, B. Dunn, Energy Environ. Sci. 7 (2014) 1597–1614.
[26] D.P. Dubal, O. Ayyad, V. Ruiz, P. Gomez-Romero, Chem. Soc. Rev. 44 (2015) 1777–1790.
[27] S. Zheng, Z.S. Wu, S. Wang, H. Xiao, F. Zhou, C. Sun, X. Bao, H.M. Chen, Energy Storage Mater. 6 (2017) 70–97.
[28] B. Dunn, H. Kamath, J.M. Tarascon, Science 334 (2011) 928–935.
[29] Y. Gogotsi, Nature 509 (2014) 568–570.
[30] J. Chmiola, G. Yushin, Y. Gogotsi, C. Portet, P. Simon, P.L. Taberna, Science 313 (2006) 1760–1763.
[31] G.L. Soloveichik, Nature 505 (2014) 163–165.
[32] H. Wang, H. Dai, Chem. Soc. Rev. 42 (2013) 3088–3113.
[33] C. Zhong, Y. Deng, W. Hu, J. Qiao, L. Zhang, J. Zhang, Chem. Soc. Rev. 44 (2015) 7484–7539.
[34] Y.-Z. Zhang, Y. Wang, T. Chen, W.-Y. Lai, H. Pang, W. Huang, Chem. Soc. Rev. 44 (2015) 5181–5199.
[35] N.S. Malvankar, M. Vargas, K.P. Nevin, A.E. Franks, C. Leang, B.C. Kim, K. Inoue, T. Mester, S.F. Covalla, J.P. Johnson, V.M. Rotello, M.T. Tuominen, D.R. Lovley, Nat. Nanotechnol. 6 (2011) 573–579.
[36] J. Chmiola, C. Largeot, P.L. Taberna, P. Simon, Y. Gogotsi, Science 328 (2010) 480–483.
[37] D.W. Wang, F. Li, M. Liu, G.Q. Lu, H.M. Cheng, Angew. Chem. Int. Ed. 47 (2008) 373–376.
[38] Y. Wang, C.Y. Foo, T.K. Hoo, M. Ng, J.Y. Lin, Chem. Eur. J. 16 (2010) 3598–3603.
[39] Y. Zhang, B. Wang, F. Liu, J. Cheng, X. Zhang, L. Zhang, Nano Energy 27 (2016) 627–637.
[40] G.S. Gund, D.P. Dubal, S. Shinde, C.D. Lokhande, ACS Appl. Mater. Interfaces 6 (2014) 3176–3188.
[41] X. Wu, Z. Han, X. Zheng, S. Yao, X. Yang, T. Zhai, Nano Energy 31 (2017) 410–417.
[42] G. Ye, Y. Gong, K. Keyshar, E.A.M. Husain, G. Brunetto, S. Yang, R. Vajtai, P.M. Ajayan, Part. Part. Syst. Charact. 32 (2015) 817–821.
[43] J. Chang, M. Jin, F. Yao, T.H. Kim, V.T. Le, H. Yue, F. Gunes, B. Li, A. Ghosh, S. Xie, Y.H. Lee, Adv. Funct. Mater. 23 (2013) 5074–5083.
[44] Y. Zhang, L. Li, H. Su, W. Huang, X. Dong, J. Mater. Chem. A 3 (2015) 43–59.
[45] D.P. Dubal, P. Gomez-Romero, B.R. Sankapal, R. Holze, Nano Energy 11 (2015) 377–399.
[46] G. Zhang, X.W. Lou, Adv. Mater. 25 (2013) 976–979.
[47] Q. Wang, B. Liu, X. Wang, S. Ran, L. Wang, D. Chen, G. Shen, J. Mater. Chem. 22 (2012) 21647–21653.
[48] Q.W. Ye, Y.C. Xiang, T.J. Ping, Q.Q. Zhou, Electrochim. Acta 56 (2011) 7517–7522.
[49] H. Wang, Q. Gao, L. Jiang, Small 7 (2011) 2454–2459.
[50] R. Zou, K. Xu, T. Wang, G. He, Q. Liu, X. Liu, Z. Zhang, J. Hu, J. Mater. Chem. A 1 (2013) 8560–8566.
[51] H. Jiang, J. Ma, C. Li, Chem. Commun. 48 (2012) 4465–4467.
[52] B. Cui, H. Lin, Y. Liu, J. Li, P. Sun, X. Zhao, C. Liu, J. Phys. Chem. C 113 (2009) 14083–14087.
[53] J. Zhang, Q. Mei, Y. Ding, K. Guo, X. Yang, J. Zhao, ACS Appl. Mater. Inter. 9 (2017) 29771–29781.
[54] J.F. Marco, J.R. Gancedo, M. Gracia, J.L. Gautier, E. Ríos, F.J. Berry, J. Solid State Chem. 153 (2000) 74–81.
[55] C. Yuan, J. Li, L. Hou, X. Zhang, L. Shen, X.W. Lou, Adv. Funct. Mater. 22 (2012) 4592–4597.
[56] M. Lenglet, R. Guillamet, J. Dürr, D. Gryffory, R.E. Vandenberghe, Solid State Commun. 74 (1990) 1035–1039.
[57] Z Wu, Y Zhu, X Ji, J. Mater. Chem. A 2 (2014) 14759–14772.
[58] X.Y. Liu, S.J. Shi, Q.Q. Xiong, L. Li, Y.J. Zhang, H. Tang, C.D. Du, X.L. Wang, J.P. Tu, ACS Appl. Mater. Inter. 5 (2013) 8790–8795.
[59] Y. Chen, B. Qu, L. Hu, Z. Xu, Q. Li, T. Wang, Nanoscale 5 (2013) 9812–9820.
[60] H. Jiang, J. Ma, C. Li, Chem. Commun. 48 (2012) 4465–4467.
[61] Y. Zhang, M. Ma, J. Yang, H. Su, W. Huang, X. Dong, Nanoscale 6 (2014) 4303–4308.
[62] J. Mei, T. Liao, L. Kou, Z. Sun, Adv. Mater. 29 (2017) 1700176.
[63] L. Wen, F. Li, H.-M. Cheng, Adv. Mater. 28 (2016) 4306–4337.
[64] D. Chen, Q. Wang, R. Wang, G. Shen, J. Mater. Chem. A 3 (2015) 10158–10173.
[65] L.L. Hench, J.K. West, Chem. Rev. 90 (1990) 33–72.
[66] Y.Q. Wu, X.Y. Chen, P.T. Ji, Q.Q. Zhou, Electrochim. Acta 56 (2011) 7517–7522.
[67] T.Y. Wei, C.H. Chen, H.C. Chen, S.Y. Lu, Adv. Mater. 22 (2010) 347–351.
[68] M.-C. Liu, L.-B. Kong, C. Lu, X.-M. Li, Y.-C. Luo, L. Kang, X. Li, F.C. Walsh, J. Electrochem. Soc. 159 (2012) A1262–A1266.
[69] M.-C. Liu, L.-B. Kong, C. Lu, X.-M. Li, Y.-C. Luo, L. Kang, ACS Appl. Mater. Interfaces 4 (2012) 4631–4636.
[70] F.Schüth Taguchi, Microporous Mesoporous Mater. 77 (2005) 1–45.
[71] Y. Zhang, L. Li, H. Su, W. Huang, X. Dong, J. Mater. Chem. A 3 (2015) 43–59.
[72] C. Yuan, J. Li, L. Hou, J. Lin, G. Pang, L. Zhang, L. Lian, X. Zhang, J. Mater. Chem. A 3 (2013) 18573–18578.
[73] S. Liu, S. Sun, X.-Z You, Nanoscale 6 (2014) 2037–2045.
[74] G. Lota, K. Fic, E. Frackowiak, Energy Environ. Sci. 4 (2011) 1592–1605.
[75] H.-W. Wang, Z.-A. Hu, Y.-Q. Chang, Y.-L. Chen, H.-Y. Wu, Z.-Y. Zhang, Y.-Y. Yang, J. Mater. Chem. 21 (2011) 10504–10511.
[76] M.F. El-Kady, V. Strong, S. Dubin, R.B. Kaner, Science 335 (2012) 1326–1330.
[77] L.L. Li, S.J. Peng, Y.L. Cheah, P.F. Teh, J. Wang, G. Wee, Y.W. Ko, C.L. Wong, M. Srinivasan, Chem. Eur. J. 19 (2013) 5892–5898.
[78] W. Xiong, Y. Gao, X. Wu, X. Hu, D. Lan, Y. Chen, X. Pu, Y. Zeng, J. Su, Z. Zhu, ACS Appl. Mater. Interfaces 6 (2014) 19416–19423.
[79] L. Shen, L. Yu, X.Y. Yu, X. Zhang, X.W. Lou, Angew. Chem. Int. Edit. 54 (2015) 1868–1872.
[80] X.-L. Wu, T. Wen, H.-L. Guo, S. Yang, X. Wang, A.-W. Xu, ACS Nano 7 (2013) 3589–3597.
[81] L. Li, S. Peng, Y. Cheah, P. Teh, J. Wang, G. Wee, Y. Ko, C. Wong, M. Srinivasan, CHEM-EUR. J. 19 (2013) 5892–5898.
[82] J. Yan, Y.P. Huang, Y.E. Miao, W.W. Tjiu, T.X. Liu, J. Hazard. Mater. 283 (2015) 730–739.
[83] S. Cavaliere, S. Subianto, I. Savych, D.J. Jones, J. Roziere, Energy Environ. Sci. 4 (2011) 4761–4785.
[84] P. Zhang, C. Shao, Z. Zhang, M. Zhang, J. Mu, Z. Guo, Y. Liu, Nanoscale 3 (2011) 3357–3363.
[85] C. Kim, K.S. Yang, Appl. Phys. Lett. 83 (2003) 1216–1218.
[86] Y.P. Huang, Y.E. Miao, L.S. Zhang, W.W. Tjiu, J.S. Pan, T.X. Liu, Nanoscale 6 (2014) 10673–10679.
[87] J. Wang, Y. Yang, Z. Huang, F. Kang, Electrochim. Acta 56 (2011) 9240–9247.
[88] M.J. Zhi, A. Manivannan, F.K. Meng, N.Q. Wu, J. Power Sources 208 (2012) 345–353.
[89] Y.P. Huang, Y.E. Miao, W.W. Tjiu, T.X. Liu, RSC Adv. 5 (2015) 18952–18959.
[90] F. Lai, Y.E. Miao, Y Huang, T.-S. Chung, T. Liu, J. Phys. Chem. C 119 (2015) 13442–13450.
[91] M. Musiani, Electrochim. Acta 45 (2000) 3397–3402.
[92] J. Du, G. Zhou, H. Zhang, C. Cheng, J. Ma, W. Wei, L. Chen, T. Wang, ACS Appl. Mater. Interfaces 5 (2013) 7405–7409.
[93] Y. An, Z. Hu, B. Guo, N. An, Y. Zhang, Z. Li, Y. Yang, H. Wu, RSC Adv. 6 (2016) 37562–37573.
[94] Y. Liu, Y. Jiao, Z. Zhang, F. Qu, A. Umar, X. Wu, ACS Appl. Mater. Interfaces 6 (2014) 2174–2184.
[95] J. Wu, P. Guo, R. Mi, X. Liu, H. Zhang, J. Mei, H. Liu, W.-M. Lau, L.-M. Liu, J. Mater. Chem. A 3 (2015) 15331–15338.
[96] L. Huang, D. Chen, Y. Ding, Z.L. Wang, Z. Zeng, M. Liu, ACS Appl. Mater. Interfaces 5 (2013) 11159–11162.
[97] G. Zhang, T. Wang, X. Yu, H. Zhang, H. Duan, B. Lu, Nano Energy 2 (2013) 586–594.
[98] S. Feng, R. Xu, Accounts Chem. Res. 34 (2001) 239–247.
[99] X. Zhang, X. Cheng, Q. Zhang, J. Energy Chem. 25 (2016) 967–984.
[100] J. Pu, J. Wang, X. Jin, F. Cui, E. Sheng, Z. Wang, Electrochim. Acta 106 (2013) 226–234.
[101] X.Y. Yu, X.Z. Yao, T. Luo, Y. Jia, J.H. Liu, X.J. Huang, ACS Appl. Mater. Interfaces 6 (2014) 3689–3695.
[102] R. Ding, L. Qi, M. Jia, H. Wang, J. Appl. Electrochem. 43 (2013) 903–910.
[103] X. Lai, J.E. Halpert, D. Wang, EnergyEnviron. Sci. 5 (2012) 5604–5618.
[104] Y. Zhang, M. Ma, J. Yang, H. Su, W. Huang, X. Dong, Nanoscale 6 (2014) 4303–4308.
[105] J. Wang, Y. Zhang, J. Ye, H. Wei, J. Hao, J. Mu, S. Zhao, S. Hussain, RSC Adv. 6 (2016) 70077–70084.
[106] C. Yuan, J. Li, L. Hou, J. Lin, X. Zhang, S. Xiong, J. Mater. Chem. A 1 (2013) 11145–11151.
[107] C.T. Hsu, C.C. Hu, J. Power Sources 242 (2013) 662–671.
[108] C. An, Y. Wang, Y. Huang, Y. Xu, C. Xu, L. Jiao, H. Yuan, CrystEngComm 16 (2014) 385–392.
[109] M. Rui, X. Li, L. Gan, T. Zhai, H. Zeng, Adv. Funct. Mater. 26 (2016) 5051–5060.
[110] S. Buller, J. Strun, J. Energy Chem. 25 (2016) 171–190.
[111] G. Zhang, X. Xiao, B. Li, P. Gu, H. Xue, H. Pang, J. Mater. Chem. A 5 (2017) 8155–8186.
[112] Y. Liu, X. Peng, Appl. Mater. Today 8 (2017) 104–115.
[113] B.X. Li, Y.F. Wang, J. Phys. Chem. C 114 (2010) 890–896.
[114] G. Zhang, L. Yu, H.E. Hoster, X.W. Lou, Nanoscale 5 (2013) 877–881.
[115] C. Tang, M.-M. Titirici, Q. Zhang, J. Energy Chem. 26 (2017) 1077–1093.
[116] Y. Li, L. Kong, M. Liu, W. Zhang, L. Kang, J. Energy Chem. 26 (2017) 494–500.
[117] X. Wang, X.L. Wu, Y.G. Guo, Y. Zhong, X. Cao, Y. Ma, J. Yao, Adv. Funct. Mater. 20 (2010) 1680–1686.
[118] D. Ge, L. Yang, Z. Tong, Y. Ding, W. Xin, J. Zhao, Y. Li, Electrochim. Acta 104 (2013) 191–197.

[119] J. Liang, Z. Fan, S. Chen, S. Ding, G. Yang, Chem. Mater. 26 (2014) 4354–4360.
[120] X.F. Lu, D.J. Wu, R.Z. Li, Q. Li, S.H. Ye, Y.X. Tong, G.R. Li, J. Mater. Chem. A 2 (2014) 4706–4713.
[121] C. Ji, F. Liu, L. Xu, S. Yang, J. Mater. Chem. A 5 (2017) 5568–5576.
[122] A.L.M. Reddy, S.R. Gowda, M.M. Shaijumon, P.M. Ajayan, Adv. Mater. 24 (2012) 5045–5064.
[123] H. Zhang, D. Xiao, Q. Li, Y. Ma, S. Yuan, L. Xie, C. Chen, C. Lu, J. Energy Chem. 27 (2018) 195–202.
[124] H.Y. Wu, H.W. Wang, Acta Phys. Chim. Sin. 29 (2013) 1501–1506.
[125] H. Zhao, L. Liu, R. Vellacheri, Y. Lei, Adv. Sci. 4 (2017) 1700188.
[126] J. Du, G. Zhou, H.M. Zhang, C. Cheng, J.M. Ma, W.F. Wei, L.B. Chen, T.H. Wang, ACS Appl. Mater. Interfaces 5 (2013) 7405–7409.
[127] R.J. Zou, K.B. Xu, T. Wang, G.J. He, Q. Liu, X.J. Liu, Z.Y. Zhang, J.Q. Hu, J. Mater. Chem. A 1 (2013) 8560–8566.
[128] Wu C, J. Cai, Y. Zhu, K. Zhang, RSC Adv. 6 (2016) 63905–63914.
[129] X. Liu, S. Shi, Q. Xiong, L. Li, Y. Zhang, H. Tang, C. Gu, X. Wang, J. Tu, ACS Appl. Mater. Interfaces 5 (2013) 8790–8795.
[130] H. Jiang, J. Ma, C.Z. Li, Chem. Commun. 48 (2012) 4465–4467.
[131] Q.F. Wang, X.F. Wang, B. Liu, G. Yu, X.J. Hou, D. Chen, G.Z. Shen, J. Mater. Chem. A 1 (2013) 2468–2473.
[132] C. Guan, X.H. Xia, N. Meng, Z.Y. Zeng, X.H. Cao, C. Soci, H. Zhang, H.J. Fan, Energy Environ. Sci. 5 (2012) 9085–9090.
[133] J.P. Liu, J. Jiang, C.W. Cheng, H.X. Li, J.X. Zhang, H. Gong, H.J. Fan, Adv. Mater. 23 (2011) 2076–2081.
[134] S. Chen, G. Yang, Y. Jia, H. Zheng, J. Mater. Chem. A 5 (2017) 1028–1034.
[135] D.P. Cai, B. Liu, D.D. Wang, L.L. Wang, Y. Liu, H. Li, Y.R. Wang, Q.H. Li, T.H. Wang, J. Mater. Chem. A 2 (2014) 4954–4960.
[136] C. Cui, L.Wang Xu, D. Guo, M. Mao, J. Ma, T. Wang, ACS Appl. Mater. Interfaces 8 (2016) 8568–8575.
[137] Z. Gu, X. Zhang, J. Mater. Chem. A 4 (2016) 8249–8254.
[138] Y. Yuan, W. Wang, J. Yang, H. Tang, Z. Ye, Y. Zeng, J. Lu, Langmuir 33 (2017) 10446–10454.
[139] L. Hu, L. Wu, M. Liao, X. Fang, Adv. Mater. 23 (2011) 1988–1992.
[140] J.M. Choi, S. Im, Applied Surf. Sci. 244 (2005) 435–438.
[141] B. Li, Y. Wang, J. Phys. Chem. C 114 (2010) 890–896.
[142] R.V. Kumar, Y. Diamant, A. Gedanken, Chem. Mater. 12 (2000) 2301–2305.
[143] Z.R. Tian, W. Tong, J.Y. Wang, N.G. Duan, V.V. Krishnan, S.L. Suib, Science 276 (1997) 926–930.
[144] Y. Rao, D.M. Antonelli, J. Mater. Chem. 19 (2009) 1937–1944.
[145] M. Cabo, E. Pellicer, E. Rossinyol, M. Estrader, A. Lopez-Ortega, J. Nogues, O.E. Castell, S. Surinach, M.D. Baro, J. Mater. Chem. 20 (2010) 7021–7028.
[146] M. Dai, L. Song, J.T. LaBelle, B.D. Vogt, Chem. Mater. 23 (2011) 2869–2878.
[147] J.W. Lee, T. Ahn, D. Soundararajan, J.M. Ko, J.D. Kim, Chem. Commun. 47 (2011) 6305–6307.
[148] C. Sassoye, C. Laberty, H. Le Khanh, C. Sophie, B. Cédric, A. Markus, S. Clément, Adv. Funct. Mater. 19 (2009) 1922–1929.
[149] L.Q. Mai, F. Yang, Y.L. Zhao, X. Xu, Y.Z. Zhao, Nat. Commun. 2 (2011) 381.
[150] J. Liu, Y. Li, X. Huang, G. Li, Z. Li, Adv. Funct. Mater. 18 (2008) 1448–1458.
[151] D. Zhao, W. Zhou, H. Li, Chem. Mater. 19 (2007) 3882–3891.
[152] G.W. Yang, C.L. Xu, H.L. Li, Chem. Commun. 48 (2008) 6537–6539.
[153] N. Fertig, M. George, M. George, R.H. Blick, J.C. Behrends, Appl. Phys. Lett. 81 (2002) 4865–4867.
[154] G.R. Fu, Z.A. Hu, L.J. Xie, X.Q. Jin, Y.L. Xie, Y.X. Wang, Z.Y. Zhang, Y.Y. Yang, H.Y. Wu, Int. J. Electrochem. Sci. 4 (2009) 1052–1062.
[155] J.H. Kim, S.H. Kang K. Zhu, J.Y. Kim, N.R. Neale, A. Frank, J. Chem. Commun. 47 (2011) 5214–5216.
[156] L. Yu, G. Zhang, C. Yuan, X.W. Lou, Chem. Commun. 49 (2013) 137–139.
[157] W. Zhou, D. Kong, X. Jia, C. Ding, C. Cheng, G. Wen, J. Mater. Chem. A 2 (2014) 6310–6315.
[158] X. Liu, S. Shi, Q. Xiong, L. Li, Y. Zhang, H. Tang, C. Gu, X. Wang, J. Tu, ACS Appl. Mater. Interfaces 5 (2013) 8790–8795.
[159] W. Yang, Z. Gao, J. Ma, X. Zhang, J. Liu, J. Materials Chem. A 2 (2014) 1448–1457.
[160] P. Sennu, V. Aravindan, Y.S. Lee, J. Power Sources 306 (2016) 248–257.
[161] F. Bao, Z. Zhang, W. Guo, X. Liu, Electrochim. Acta 157 (2015) 31–40.
[162] B.E. Conway, V. Birss, J. Wojtowicz, J. Power Sources 66 (1997) 1–14.
[163] E. Frackowiak, V. Khomenko, K. Jurewicz, K. Lota, F. Béguin, J. Power Sources 153 (2006) 413–418.
[164] A.J. Heeger, Rev. Mod. Phys. 73 (2001) 681–700.
[165] K. Wang, H. Wu, Y. Meng, Z. Wei, Small 10 (2014) 14–31.
[166] Q. Wang, X. Wang, B. Liu, G. Yu, X. Hou, D. Chen, G. Shen, J. Mater. Chem. A 1 (2013) 2468–2473.
[167] G.Q. Zhang, H.B. Wu, H.E. Hoster, M.B. Chan-Park, X.W. Lou, Energy Environ. Sci. 5 (2012) 9453–9456.
[168] X. Peng, K.F. Huo, J.J. Fu, X.M. Zhang, B. Gao, P.K. Chu, Chem. Commun. 49 (2013) 10172–10174.
[169] K. Xu, X. Huang, Q. Liu, R. Zou, W. Li, X. Liu, S. Li, J. Yang, J. Hu, J. Mater. Chem. A 2 (2014) 16731–16739.
[170] J. Pu, F.L. Cui, S.B. Chu, T.T. Wang, E.H. Sheng, Z.H. Wang, ACS Sustain. Chem. Eng. 2 (2013) 809–815.
[171] Y. Yan, T. Wang, X. Li, H. Pang, H. Xue, Inorg. Chem. Front. 4 (2017) 33–51.
[172] D. Kong, W. Ren, C. Cheng, Y. Wang, Z. Huang, H.Y. Yang, ACS Appl. Mater. Interfaces 7 (2015) 21334–21346.
[173] K. Wang, J. Huang, Z. Wei, J. Phys. Chem. C 114 (2010) 8062–8067.
[174] N. Jabeen, Q. Xia, M. Yang, H. Xia, ACS Appl. Mater. Interfaces 8 (2016) 6093–6100.
[175] W. Zhang, H. Pang W. Sun, Y.Wang L.-Ping, Electrochem. Commun. 87 (2017) 80–85.
[176] D.Y. Lee, S.J. Yoon, N.K. Shrestha, S.-H. Lee, H. Ahn, S.-H. Han, Microporous Mesoporous Mater. 153 (2012) 163–165.
[177] J. Zhou, B. Wang, Chem. Soc. Rev. 46 (2017) 6927–6945.
[178] H. Furukawa, K.E. Cordova, M. O'Keeffe, O.M. Yaghi, Science 341 (2013) 1230444.
[179] A.P. Cote, A.I. Benin, N.W. Ockwig, M. O'Keeffe, A.J. Matzger, O.M. Yaghi, Science 310 (2005) 1166–1170.
[180] C.V. McGuire, R.S. Forgan, Chem. Commun. 51 (2015) 5199–5217.
[181] S.L. James, Chem. Soc. Rev. 32 (2003) 276–288.
[182] I. Stassen, M. Styles, G. Grenci, H.V. Gorp, W. Vanderlinden, S.D. Feyter, P. Falcaro, D.D. Vos, P. Vereecken, R. Ameloot, Nat. Mater. 15 (2015) 304–310.
[183] W.J. Li, M. Tu, R. Cao, R.A. Fischer, J. Mater. Chem. A 4 (2016) 12356–12369.
[184] Z.-H. Yan, D. Li, X.-B. Yin, Sci. Bull. 62 (2017) 1344–1354.
[185] Y. Liu, H. Dong, F. Hu, Y.S. Zhao, Sci. Bull. 62 (2017) 3–4.
[186] L. Wang, X. Feng, L. Ren, Q. Piao, J. Zhong, Y. Wang, H. Li, Y. Chen, B. Wang, J. Am. Chem. Soc. 137 (2015) 4920–4923.
[187] K.M. Choi, H.M. Jeong, J.H. Park, Y.B. Zhang, J.K. Kang, O.M. Yaghi, ACS Nano 8 (2014) 7451–7457.
[188] J. Liu, C. Wu, D. Xiao, P. Kopold, L. Gu, P.A. van Aken, J. Maier, Y. Yu, Small 12 (2016) 2354–2364.
[189] H. Furukawa, K.E. Cordova, M. O'Keeffe, O.M. Yaghi, Science 341 (2013) 1230444.
[190] C.V. McGuire, R.S. Forgan, Chem. Commun. 51 (2015) 5199–5217.
[191] H.-C. Zhou, S. Kitagawa, Chem. Soc. Rev. 43 (2014) 5415–5418.
[192] W. Xia, A. Mahmood, R. Zou, Q. Xu, Energy Environ. Sci. 8 (2015) 1837–1866.
[193] Z. Jiang, Z. Li, Z. Qin, H. Sun, X. Jiao, D. Chen, Nanoscale 5 (2013) 11770–11775.
[194] C. Sun, J. Yang, X. Rui, W. Zhang, Q. Yan, P. Chen, F. Huo, W. Huang, X. Dong, J. Mater. Chem. A 3 (2015) 8483–8488.
[195] S. Chen, M. Xue, Y. Li, S. Qiu, J. Mater. Chem. A 3 (2015) 20145–20152.
[196] J.K. Sun, Q. Xu, Energy Environ. Sci. 7 (2014) 2071–2100.
[197] Y. Zhao, X. Li, J. Liu, C. Wang, Y. Zhao, G. Yue, ACS Appl. Mater. Interfaces 8 (2016) 6472–6480.
[198] A. Morozan, F. Jaouen, Energy Environ. Sci. 5 (2012) 9269–9290.
[199] J. Qi, X. Lai, J. Wang, H. Tang, H. Ren, Y. Yang, Q. Jin, L. Zhang, R. Yu, G. Ma, Z. Su, H. Zhao, D. Wang, Chem. Soc. Rev. 44 (2015) 6749–6773.
[200] A. Mahmood, W. Guo, H. Tabassum, R. Zou, Adv. Energy Mater. 6 (2016) 1600423.
[201] S. Wang, J. Wang, M. Zhu, X. Bao, B. Xiao, D. Su, H. Li, Y. Wang, J. Am. Chem. Soc. 137 (2015) 15753–15759.
[202] L. Shang, H. Yu, X. Huang, T. Bian, R. Shi, Y. Zhao, G.I. Waterhouse, L.Z. Wu, C.H. Tung, T. Zhang, Adv. Mater. 28 (2015) 1668–1674.
[203] S. Mao, Z. Wen, T. Huang, Y. Hou, J. Chen, Energy Environ. Sci. 7 (2014) 609–616.
[204] C. Sun, J. Yang, X. Rui, W. Zhang, Q. Yan, P. Chen, F. Huo, W. Huang, X. Dong, J. Mater. Chem. A 3 (2015) 8483–8488.
[205] R. Díaz, M.G. Orcajo, J.A. Botas, G. Calleja, J. Palma, Mater. Lett. 68 (2012) 126–128.
[206] H. Wang, Q.L. Zhu, R. Zou, Q. Xu, Chem. 2 (2017) 52–80.
[207] K.M. Choi, H.M. Jeong, J.H. Park, Y.-B. Zhang, J.K. Kang, O.M. Yaghi, ACS Nano 8 (2014) 7451–7457.
[208] X.Y. Yu, L. Yu, H.B. Wu, X.W. Lou, Angew. Chem. 127 (2015) 5421–5425.
[209] D.Y. Lee, D.V. Shinde, E.-K. Kim, W. Lee, I.-W. Oh, N.K. Shrestha, J.K. Lee, S.-H. Han, Microporous Mesoporous Mater. 171 (2013) 53–57.
[210] L. Wang, X. Feng, L. Ren, Q. Piao, J. Zhong, Y. Wang, H. Li, Y. Chen, B. Wang, J. Am. Chem. Soc. 137 (2015) 4920–4923.
[211] L. Zhang, H.B. Wu, X.W. Lou, J. Am. Chem. Soc. 135 (2013) 10664–10672.
[212] Z. Liu, C. Liu, J. Ya, E. Lei, Renew. Energy 36 (2011) 1177–1181.
[213] J. Yang, Y. Lin, Y. Meng, Y. Liu, Ceram. Int. 38 (2012) 4555–4559.
[214] X. Gan, X. Li, X. Gao, W. Yu, J. Alloys Compd. 481 (2009) 397–401.
[215] W. Zeng, L. Wang, H. Shi, G. Zhang, K. Zhang, H. Zhang, F. Gong, T. Wang, H. Duan, J. Mater. Chem. A 4 (2016) 8233–8241.
[216] C. Guan, X. Liu, W. Ren, X. Li, C. Cheng, J. Wang, Adv. Energy Mater. 7 (2017) 1602391.
[217] H. Hu, B. Guan, B. Xia, X.W. Lou, J. Am. Chem. Soc. 137 (2015) 5590–5595.
[218] H. Li, M. Eddaoudi, M. O'Keeffe, O.M. Yaghi, Nature 402 (1999) 276–279.
[219] J. Jiang, Y. Li, J. Liu, X. Huang, C. Yuan, X.W. (David) Lou, Adv. Mater. 43 (2015) 5166–5180.
[220] Y. Yang, D. Cheng, S. Chen, Y. Guan, J. Xiong, Electrochim. Acta 193 (2016) 116–127.
[221] Y.P. Gao, K.J. Huang, Chem. Asian J. 12 (2017) 1969–1984.
[222] W. Zhou, X. Cao, Z. Zeng, W. Shi, Y. Zhu, Q. Yan, H. Liu, J. Wang, H. Zhang, Energy Environ. Sci. 6 (2013) 2216–2221.
[223] X. Xia, C. Zhu, J. Luo, C.Guan Z. Zeng, C.F. Ng, Small 10 (2014) 766–773.
[224] Q. Chu, W. Wang, X. Wang, B. Yang, X. Liu, J. Chen, J. Power Sour. 276 (2015) 19–25.
[225] B. Liu, D. Kong, Z.X. Huang, R. Mo, Y. Wang, Z. Han, C. Cheng, H.Y. Yang, Nanoscale 8 (2016) 10686–10694.
[226] J. Wang, S. Wang, Z. Huang, Y. Yu, J. Mater. Chem. A 2 (2014) 17595–17601.
[227] Y. Liu, S. Wen, W. Shi, Mater. Lett. 214 (2018) 194–197.
[228] L.N. Wang, Y. Ma, M. Yang, Y.X. Qi, Electrochim. Acta 186 (2015) 391–396.
[229] S. Wen, Y. Liu, F. Zhu, R. Shao, W. Xu, Appl. Surf. Sci. 428 (2018) 616–622.
[230] L.B. Ma, Y. Hu, R.P. Chen, G.Y. Zhu, T. Chen, H.L. Lv, Y.R. Wang, J. Liang, H.X. Liu, C.Z. Yan, H.F. Zhu, Z.X. Tie, Z. Jin, J. Liu, Nano Energy 24 (2016) 139–147.

[231] H. Chen, X.L. Liu, J.M. Zhang, F. Dong, Y.X. Zhang, Ceram. Int. 42 (2016) 8909–8914.
[232] C. Xia, P. Li, A.N. Gandi, U. Schwingenschlogl, H.N. Alshareef, Chem. Mater. 27 (2015) 6482–6485.
[233] S. Raj, S.K. Srivastava, P. Kar, P. Roy, RSC Adv. 6 (2016) 95760–95767.
[234] X. Li, B. Wei, Nano Energy 2 (2013) 159–173.
[235] T. Chen, L. Dai, Mater. Today 16 (2013) 272–280.
[236] X. Shi, S. Zheng, Z.-S. Wu, X. Bao, J. Energy. Chem. 27 (2018) 25–42.
[237] S. Abouali, M.A. Garakani, Z.L. Xu, J.K. Kim, Carbon 102 (2016) 262–272.
[238] J. Yang, C. Yu, S. Liang, S. Li, H. Huang, X. Han, C. Zhao, X. Song, C. Hao, J. Qiu, Chem. Mater. 28 (2016) 5855–5863.
[239] S. Sun, S. Wang, S. Li, Y. Li, Y. Zhang, J. Chen, Z. Zhang, S. Fang, P. Wang, J. Mater. Chem. A 4 (2016) 18646–18653.
[240] G.A.M. Ali, S.A.A. Manaf, A. Divyashree, K.F. Chong, G. Hegde, J. Energy Chem. 25(2016) 734–739.
[241] Y. Xu, L. Wang, P. Cao, C. Cai, Y. Fu, X. Ma, J. Power Sources 306 (2016) 742–752.
[242] L. Zhang, L. Dong, M. Li, P. Wang, J. Zhang, H. Lu, J. Mater. Chem. A 6 (2018) 1412–1422.
[243] S. Sun, S. Li, S. Wang, Y. Li, L. Han, H. Kong, P. Wang, Mater. Lett. 182 (2016) 23–26.
[244] W. Li, F. Yang, Z. Hu, Y. Liu, J. Alloys Compounds 749 (2018) 305–312.
[245] X. Li, W. Sun, L. Wang, Y. Qi, T. Guo, X. Zhao, X. Yan, RSC Adv. 5 (2015) 7976–7985.
[246] L. Huang, W. Zhang, J. Xiang, Y. Huang, J. Materiomics 2 (2016) 248–255.